ChemComm

REVIEW ARTICLE

View Article Online
View Journal

Cite this: DOI: 10.1039/d5cc07133j

Cold plasma deposited thin-film nanocomposites for heterogeneous thermocatalysis – concepts and progress

Jacek Tyczkowski * and Hanna Kierzkowska-Pawlak

There is no doubt that the development of chemical technologies is closely tied to progress in catalysis. Two aspects are crucial here: the search for new, efficient, selective, and stable nanocatalysts tailored to specific reactions and obtaining them in forms best suited for modern catalytic systems, such as structured reactors. Both challenges fit perfectly within the capabilities of cold (non-equilibrium) plasma thin-film deposition technology. The enormous potential of this technology for producing new nanocomposite materials with predetermined molecular structures, nanostructures, and electronic structures that are so crucial for catalytic properties seems unrivaled. This review summarizes recent progress in cold plasma deposition methods, including low-pressure plasma-enhanced chemical vapor deposition (PECVD), atmospheric-pressure plasma deposition (APPD), and plasma-enhanced atomic layer deposition (PEALD), and highlights their usefulness in fabricating thin films on 3D supports as packings for catalytic structured reactors. Advances in plasma deposition of nanocomposite films and the design of their architectures for catalytic activity are also discussed, with particular focus on emerging research involving nanoscale heterojunctions. Furthermore, the most important chemical processes currently being tested using plasma-derived nanocatalysts are presented, providing strong evidence of their practical applicability. Overall, this work demonstrates the significant potential of cold plasma technology for the design and fabrication of innovative nanocatalysts.

Received 15th December 2025,
Accepted 21st January 2026

DOI: 10.1039/d5cc07133j

rsc.li/chemcomm

Department of Chemical and Molecular Engineering, Faculty of Process and Environmental Engineering, Lodz University of Technology, Wólczańska 213, Łódź 93-005, Poland. E-mail: jacek.tyczkowski@p.lodz.pl

Jacek Tyczkowski

Jacek Tyczkowski is a full professor of chemical engineering and a Fellow of the Alexander von Humboldt Foundation. Until 2000, he worked at the Centre of Molecular and Macromolecular Studies of the Polish Academy of Sciences and subsequently joined the Lodz University of Technology. He held a postdoctoral fellowship at the Philipps University of Marburg and has served as a visiting professor at universities such as TU Wien and twice at Shizuoka University (RIE in Hamamatsu). His research focuses on molecular engineering, particularly plasma chemistry and the physicochemistry (including electronic properties) of plasma-produced thin films and nanostructures.

Hanna Kierzkowska-Pawlak

Hanna Kierzkowska-Pawlak is a full professor of chemical engineering at the Faculty of Process and Environmental Engineering, Lodz University of Technology, where she leads the Division of Molecular Engineering. From 2016 to 2017, she was a visiting researcher at Shizuoka University (Japan). Her research focuses on catalytic CO_2 conversion to value-added chemicals and advancing absorption technologies for CO_2 capture. She is an expert in cold plasma methods for the fabrication of new thin-film nanocatalysts for environmental applications and applies plasma techniques to material surface engineering. Her work integrates molecular engineering and catalysis for sustainable environmental technologies.

1. Introduction

It has long been recognized that the development of the chemical industry is strongly dependent on catalysts, without which approximately 90% of current industrial chemical processes would not be feasible.[1,2] The introduction of new technologies, as well as the pursuit of increased performance and reduced costs of those already in use, requires intensive efforts to develop increasingly advanced and effective catalytic systems. Despite the enormous progress in catalyst research, these efforts still contain an element of mystery, resembling ''alchemy'' with its ''trial-and-error'' strategy rather than the rational design of catalytic structures with predetermined properties.[3]

In the early 1990s, when the term ''nanocatalysts'' emerged, particular attention was focused on small, nanosized objects that, due to their high surface-to-volume ratio, were expected to provide significantly higher process performance relative to the amount of catalyst used. However, it was quickly realized that the transition from macroscopic to nanoscale materials not only increases the active surface area of the catalyst at a constant mass but, more importantly, can dramatically – and nonlinearly with changes in surface area – alter the catalytic activity of the resulting material, sometimes leading to unexpected and unique properties.[4,5] In some cases, materials that exhibited no catalytic activity in their bulk form became catalytically active once reduced to the nanoscale.[6] Since then, the use of nanosized catalysts in various chemical processes has generated significant interest – both in their synthesis and in the study of their catalytic properties – leading to the establishment of nanocatalysis as a major discipline in the 21st century.[7]

Focusing our considerations on heterogeneous thermocatalysis, which is the subject of this work, and setting aside other forms of catalysis such as photocatalysis or electrocatalysis, it can be stated that a breakthrough in the development of nanocatalysis in this field occurred when it was realized that not only the size but also the interactions between different materials in nanostructured forms have a profound impact on catalytic behavior. These interactions can result in properties that differ radically from those of the individual nanomaterials in isolation. Various nanocomposite structures – including nanohybrids,[8,9] as well as more specific systems such as metal–support (oxide) and oxide–support (metal) catalysts,[10,11] or single-atom and nanoparticle-single-atom catalysts[12–14] – have become the subject of extensive research. Despite significant progress, a detailed understanding of the interactions between nanocomposite components and the mechanisms of catalytic reactions occurring within such systems remains limited. The complex interactions between these components – believed to either enhance or, conversely, diminish catalytic activity – are often collectively described under the vague terms ''synergy''[15,16] and its opposite ''anti-synergy'',[17,18] leaving the relationship between catalytic properties and component interactions still largely unresolved. This situation poses yet another challenge: the rational design and fabrication of nanostructures that meet specific catalytic requirements.

Among the many methods explored for the synthesis of heterogeneous nanocatalysts,[19,20] cold (non-equilibrium) plasma deposition methods – of which the oldest and most widely used one is plasma-enhanced chemical vapor deposition (PECVD) – have been relatively neglected so far, even though they offer significant opportunities to control both the molecular structure and nanostructure and, consequently, the electronic structure of the resulting materials. Although cold plasma has already found some applications in heterogeneous catalyst technology, it has been used mainly to assist conventional synthesis routes or to modify existing catalysts, whereas the still-innovative method of direct plasma deposition remains largely underexplored.[21–25]

The cold plasma deposition technology opens new possibilities for producing nanocatalytic materials, often with unique properties unattainable by other means. The potential of this approach is enormous – perhaps limited only by our imagination and the laws of physical chemistry – and molecular engineering is increasingly employed to design material structures.[26]

Two key attributes of this technology determine its considerable potential, and it still awaits broader utilization in the rational design of nanocatalysts. First, it enables the fabrication of materials in the form of very thin films (typically < 1 μm) on virtually any substrate without altering its original geometry – an invaluable advantage in the design of structured chemical reactors. Second, it offers exceptional control over the structure of the deposited material, providing the freedom to tailor it to specific catalytic properties. It is also worth emphasizing that the synthesis of nanocatalysts using cold plasma fully aligns with the principles of green chemistry: it is virtually waste-free, consumes minimal amounts of precursors, and is energy-efficient. At the same time, it is simple to implement and readily scalable from the laboratory to the industrial level.

In this review, we introduce the concept underlying the use of cold plasma technology to fabricate thin-film nanocomposites for heterogeneous thermocatalysis, present the current state of knowledge in this field, and outline the future prospects of this approach, which is based primarily on PECVD, but also on APPD (atmospheric pressure plasma deposition) and PEALD (plasma-enhanced atomic layer deposition) methods. We begin with an introduction to this topic (Section 2) and a review of current progress (Section 3). Next, we demonstrate the possibilities of tailoring the molecular structure, nanostructure, and electronic structure of the deposited films (Section 4), followed by a discussion of correlations between the controlled structure of thin-film nanocomposites and the thermocatalytic processes occurring on them (Section 5). Finally, we summarize the broad prospects that lie ahead and encourage deeper engagement with this emerging research area (Section 6).

2. Cold plasma deposition – a bit of history

The adventure with thin films deposited in cold plasma began over 150 years ago, when the formation of solid products during

an electrical discharge in gaseous acetylene was reported.[27,28] This phenomenon – later observed in various studies involving discharges in gases containing organic compounds – was long regarded as nothing more than a curiosity, associated merely with undesirable by-products of reactions occurring in electrical discharges. It was not until the early 1960s, after the use of a plasma-deposited styrene film as an insulation layer in nuclear batteries,[29] that interest in such materials was rekindled.

From that time on, numerous publications and monographs have appeared on thin films deposited in cold plasma – their properties, structure, formation mechanisms, and potential technological applications.[30] Initially, and for a long time thereafter, these films were referred to as plasma polymers, and the process of their production was called plasma polymerization.[31] This terminology stemmed from the fact that conventional monomers were used as precursors for deposition. However, it was soon realized that virtually all organic, metal–organic, and even some inorganic compounds could serve as precursors, provided that they could be introduced into the discharge chamber in the form of a gas or vapor.[32,33] Over time, the process began to be referred to as plasma-enhanced chemical vapor deposition (PECVD), a term that can be somewhat misleading, because the mechanisms of film deposition under cold-plasma conditions differ drastically from those of high-temperature thermal CVD.[34,35]

The growing interest in the PECVD method was related to the aforementioned (Introduction) virtually unlimited ability to produce new materials in the form of thin films with controlled thickness (from a few nanometers to at most several micrometers) and often unique structures and properties. The relative simplicity of producing such films was also important, as was the more recent recognition of PECVD as an environmentally friendly method aligned with the principles of green chemistry.[36,37]

It must be acknowledged that it was initially exciting simply to introduce a selected low-molecular-weight compound into the plasma reactor and, by adjusting the process parameters, obtain a film to be examined by all available characterization techniques. However, as more applications emerged, researchers were compelled to adopt a more rational approach. With a specific application and the associated property requirements in mind, a suitable structure was designed and then implemented *via* plasma deposition by selecting appropriate precursors and controlling the process parameters. Today, extensive knowledge exists on the nature of non-equilibrium (cold) plasma, the processes occurring within it, the mechanism of thin-film formation, and the methods for depositing films with predetermined characteristics.[38]

Among the features of PECVD-produced materials, thin-film properties have played a key role in their applications, enabling uses that would have been unattainable or very difficult to realize by other methods. It is therefore not surprising that early attention focused on films serving functions such as gas barriers, reverse osmosis membranes, mechanical protection layers, selective optical absorbers, corrosion resistant coatings, biocompatible layers, and hydrophobic surfaces.[39] They were also used as photovoltaic components and as active (photocatalytic and electrocatalytic) electrode coatings in fuel cells, batteries, and water-splitting systems.[40] At that time, however, there was little need to use thin-film technology in thermocatalysis, where catalysts were typically employed in fixed-bed reactors, usually in the form of powders or shaped bodies (spheres, tablets, and pellets). Cold plasma was used only occasionally in the synthesis or post-processing of such materials. Consequently, interest in applying PECVD to deposit catalytic films for thermal catalysis was sporadic and remained within the realm of basic research, with studies generally mentioning only the potential catalytic use of such films without conducting catalytic tests.[41]

Films with potential catalytic properties produced by PECVD (primarily those based on metals or their oxides) appeared in the 1980s, when metal–organic complexes began to be used more widely as precursors for plasma deposition. The limited film characterization techniques available at the time were sufficient to determine that such films contained pure metals or their oxides, and in some cases even to identify nanoparticles. Attempts were also made to co-deposit metal–organic precursors with hydrocarbons, laying the foundation for the controlled fabrication of thin-film nanocomposites rather than by depositing films solely from metal–organic precursors with fixed chemical structures.[42–46]

In fact, PECVD films produced from metal–organic precursors and explicitly dedicated as catalytic coatings for thermocatalysis became the subject of serious interest only when the need arose with the rapid development of structured packings for catalytic reactors.[47,48] The first reports on such films date back about 20 years. The research conducted at that time focused primarily on films deposited from a cobalt precursor (cobalt(I) cyclopentadienyldicarbonyl) in radio frequency plasma onto substrates such as metal plates and meshes used as structured packing elements. The films exhibited a nanocomposite structure consisting of a carbon matrix and cobalt oxide nanoparticles (CoO_x), which, with appropriate control of production parameters, formed nanocrystalline Co_3O_4 spinel.[49,50]

The films with Co_3O_4 nanoparticles obtained in this way proved to be excellent nanocatalysts for hydrocarbon combustion, exhibiting very high activity – significantly better than that of conventional catalysts such as PtRh mesh or Co foil coated with Co_3O_4 formed by oxidation.[51] Building on this success, the films were tested in a large-scale laboratory structured reactor,[52] reinforcing the view that thin-film nanocomposites produced by PECVD hold great promise as nanocatalysts for thermocatalytic applications and motivating further research in this area.

To summarize this short historical review, which introduces us to the technology of thin film deposition in cold plasma, a timeline showing the key developmental stages and conceptual evolution of cold plasma thin film deposition discussed in this review, against the backdrop of the number of publications in this field, is presented in Fig. 1. As can be seen, the subject of plasma-deposited thin-film nanocatalysts for thermocatalysis, which is the main topic of this review, only became a regular feature of the literature in 2007. A certain decline in interest

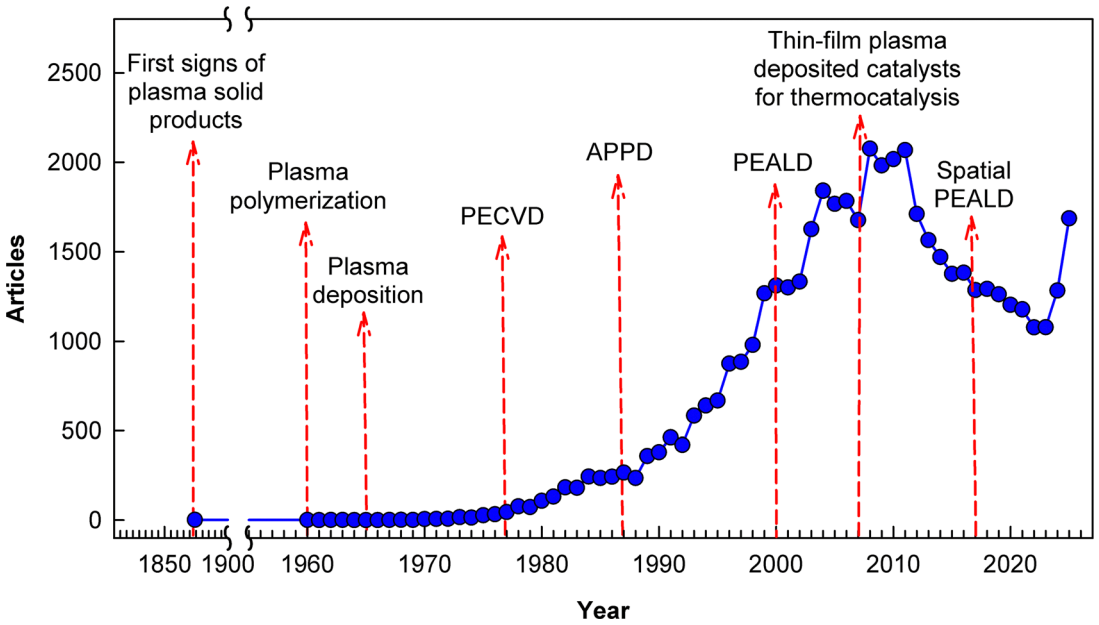

Fig. 1 A timeline showing the key developmental stages and conceptual evolution of cold plasma thin film deposition discussed in this review, against the backdrop of the number of publications on this topic. The arrows indicate the year in which a given topic became a permanent feature in the literature. The number of publications was obtained from the Scopus database and includes papers whose titles, abstracts, and keywords contained the terms "plasma polymerization", "plasma deposition", PECVD, APPD, PEALD, and their derivatives.

in plasma deposition observed after 2010 is now gaining momentum again.

3. Advances in cold plasma deposition methods

Cold plasma deposition methods for thin-film nanocomposites have advanced significantly in recent years within this rapidly evolving and promising field, opening up new and tangible opportunities for the fabrication of systems with thermocatalytic activity. Developments in plasma-enhanced chemical vapor deposition (PECVD), atmospheric pressure plasma deposition (APPD), and plasma-enhanced atomic layer deposition (PEALD), together with substantial progress in coating 3D structures and large-area substrates, provide strong impetus for the rational design and prospects of large-scale production of thin-film nanocatalysts. The distinctive features that set these catalysts apart from other catalytic materials – such as their thin-film nature and their ability to be deposited on structural substrates, which is essential for modern catalytic reactors, as well as the enormously expanding capacity to tailor molecular, nanostructural, and electronic properties, thereby ensuring the possibility of realizing the desired catalytic activity – are increasingly achievable through contemporary cold plasma deposition techniques. The following discussion highlights key advances in cold plasma deposition technology that are critical to the future development of thin-film nanocomposites with thermocatalytic activity.

3.1. Plasma-enhanced chemical vapor deposition (PECVD)

To date, the most commonly used type of cold plasma for thin film deposition is a glow discharge generated under reduced pressure in reactors with internal electrodes, *i.e.*, capacitively coupled, usually at radio frequency (most often 13.56 MHz). An example diagram of such a reactor is shown in Fig. 2a. In general, the reactor chamber is initially evacuated to 10^{-1}–10^{-3} Pa, after which a volatile precursor and often an inert carrier gas (*e.g.*, argon) are introduced into it with a controlled flow. The precursor can be any gaseous chemical compound, or it can be a sublimating solid or evaporating liquid. The role of the carrier gas is, on the one hand, to enable plasma generation in the presence of low vapor pressure precursors, and on the other, to provide control over the process of ion bombardment (*e.g.*, by Ar^+ ions) during deposition, which is crucial for shaping the structure of the growing film. Once the desired conditions are achieved in the reactor chamber (gas flow rate and partial pressures), a glow discharge is generated between the electrodes by applying an appropriate voltage. As a result of chemical processes occurring both in the gas phase of the plasma and its interaction with surfaces within its range of influence (electrodes and substrates), a thin solid film is formed on these surfaces, with a structure closely related to the type of reaction gases used and the parameters of the deposition process.[38,53]

Of course, the reactor design presented above and the procedure for deposition of thin films in it are constantly being developed and modified, covering other ranges of plasma generation frequencies (from DC discharge, through kilohertz (audio), megahertz (radio), up to microwaves), other generation conditions (*e.g.*, inductive coupling, remote plasma, presence of a magnetic field (magnetron)) or the use of glow discharge (*i.e.*, still cold plasma) at atmospheric pressure. Progress in the PECVD technique has been ongoing for many years, but new and interesting solutions continue to emerge in this field,

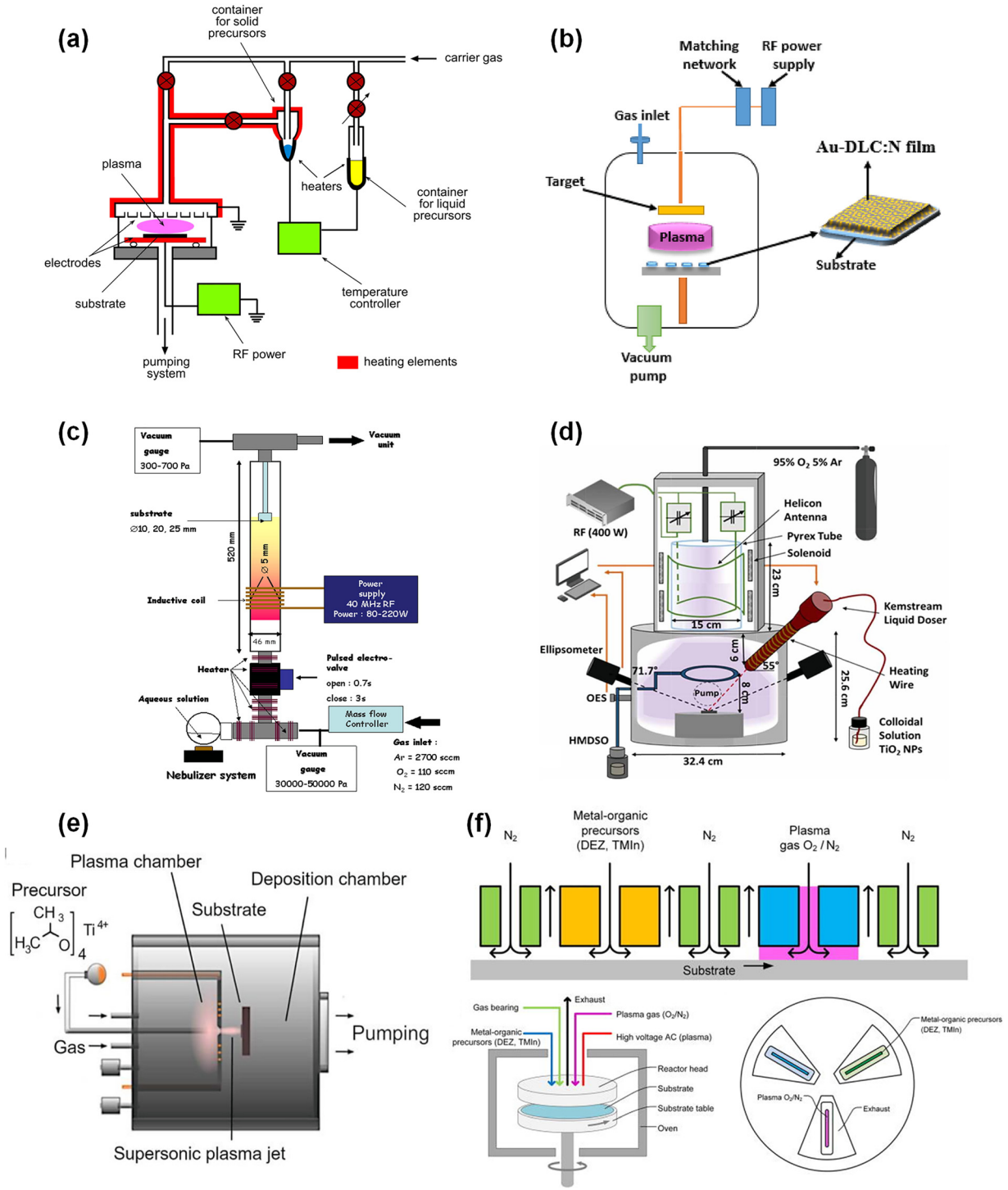

Fig. 2 Example schematics of cold plasma deposition devices: (a) a typical PECVD reactor, reproduced from ref. 26 with permission from Elsevier, copyright 2019. (b) Setup for hybrid PECVD + sputtering, reproduced from ref. 62 with permission from Elsevier, copyright 2024. (c) A PECVD reactor with precursor injection in the form of an aqueous solution, reproduced from ref. 67 with permission from Elsevier, copyright 2011. (d) A PECVD reactor with precursor injection in the form of a suspension, reproduced from ref. 69 with permission from IOP Publishing, copyright 2021. (e) Two-chamber thermal plasma/cold plasma reactor.[74] (f) Spatial PEALD concept and schematic of a wafer rotating reactor, reproduced from ref. 86 with permission from AIP Publishing, copyright 2018.

mainly aimed at achieving greater control over the deposition process and deposit uniformity, as well as shortening the process time and increasing the surface area of coated substrates.[54–57]

However, bearing in mind the use of PECVD for the production of thin nanocomposite films with potential application as nanocatalysts for thermocatalysis, further considerations will

focus mainly on relatively new and particularly important solutions that hold great promise in this field. The first innovation of this type, the foundations of which were reported quite a long time ago,[42] is the deposition of films not from one, but from two or more precursors, appropriately selected in terms of their chemical structure and content in the reaction mixture.[58,59] This approach significantly expands the possibilities for achieving the designed film structure. The co-deposition procedure can be carried out by directly feeding the precursor mixture into the reactor chamber (Fig. 2a),[26] or by introducing them separately at different locations into the plasma region, thus controlling the course of chemical reactions in the plasma more precisely.[60]

Recently, co-deposition using a combination of two techniques – PECVD and simultaneous sputtering – which was already reported some time ago,[30] has also attracted increasing attention. A schematic setup for such a ''hybrid PECVD + sputtering'' system is shown in Fig. 2b. In this way, it is possible to produce films consisting of a suitable matrix obtained in the plasma deposition process and metal nanoparticles,[61,62] or, for example, their oxides[63] or carbides.[64,65] This method offers great opportunities for direct control of the size of nanoparticles and their distribution in the film, making it a potentially useful tool for the production of designed nanocomposite structures with catalytic properties.

Despite the wide range of precursors that can be used in PECVD processes, there is a clear limitation stemming from the need for volatility (gases or vapors) and stability. Therefore, if a chemical compound is a non-subliming solid or one that can be obtained in a volatile form but undergoes rapid decomposition, we cannot use it in PECVD, even though it would be well suited to our molecular design. This inconvenience has been recognized for a long time, but only in recent years has there been some progress in this area.

One advantageous alternative is the direct injection of colloidal solutions or suspensions in the form of an aerosol into the plasma reactor chamber. In this way, non-volatile or unstable precursors can be introduced into the plasma generated in a working gas and/or a volatile precursor.[66] This method was used in the case of introducing cobalt atoms into the plasma by injecting an aqueous solution of cobalt nitrate,[67] or a hexane solution of dicobalt octacarbonyl ($Co_2(CO)_8$), which, although it boils at 325 K, immediately decomposes and cannot be delivered in the gas phase to the reaction chamber.[68] The resulting thin films containing Co_3O_4 nanoparticles showed excellent catalytic activity and long-term stability for CO oxidation at room temperature. Among other things, this method has also been used to directly introduce titanium oxide nanoparticles by providing their colloidal suspension in a mixture of organic solvents.[69] Examples of schematic PECVD setups with injection of precursor solutions are shown in Fig. 2c and d.

However, apart from the significant advantage of liquid solutions enabling the direct delivery of non-volatile or unstable precursors to the plasma reactor chamber, they also have a disadvantage, similar to that associated with volatile precursors, resulting from their chemical structure. There is still a problem with freely deciding on the composition of the reaction mixture if we use chemical compounds with a pre-fixed structure. For example, when injecting an aqueous solution of $Co(NO_3)_2$ or $CoSO_4$, in addition to cobalt atoms, we can also introduce oxygen and nitrogen or sulfur atoms into the film, which are not necessarily desirable there, and the presence of H_2O is also not without significance for the structure of the deposited film. On the other hand, when injecting a suspension of cobalt itself in the form of metallic nanoparticles, it will most likely be placed in the same nanoparticle form within the film, and its atomic dispersion under cold plasma conditions is not expected.

A way to further expand the range of precursors usable in PECVD is to combine thermal (equilibrium) plasma, in which the atomization of the substances introduced there would take place, with cold (non-equilibrium) plasma, where film deposition would occur. Virtually any material introduced into a thermal plasma chamber, whether in the form of a powder, solution, or suspension, can be atomized by selecting the appropriate parameters of the process, which takes place at high working gas pressure (*e.g.*, argon), and then fed as the resulting gas mixture into a low-pressure cold plasma chamber, where film deposition will take place, for example, with the participation of PECVD supplied with additional volatile precursors.

Two-chamber thermal plasma/cold plasma (PECVD) designs are still at the conceptual stage,[70,71] although there are already several similar solutions in which, admittedly, no additional cold plasma with further precursors is generated in the second chamber, and only film deposition takes place there, but this is done under low pressure and non-equilibrium plasma conditions.[72–74] An example of a two-chamber reactor of this type is shown in Fig. 2e.

It should be noted that controlling the processes occurring in a two-chamber reactor is a serious technological challenge requiring further research. For example, the transition of the reaction mixture from the high-pressure chamber to the low-pressure chamber can generate a supersonic stream of reactants, which undoubtedly affects the structure of the deposited film.[73,74]

Although thermal plasma/PECVD designs are in their infancy, they offer significant potential for producing thin-film nanocatalysts, primarily due to the extensive possibilities of controlling the chemical structure and nanostructure of the deposited nanocomposite films.

3.2. Atmospheric pressure plasma deposition (APPD)

Considering the prospects for the use of cold plasma for the deposition of catalytic films on a larger, industrial scale, APPD should be mentioned. Although this method is characterized by much higher deposition rates than low-pressure methods and lower costs due to the lack of pumping systems, until recently it was mainly used for surface treatment rather than for the deposition of films, which were generally inhomogeneous, had many defects, and, above all, the range of structures that

could be obtained was limited and difficult to control. However, recent advances in this technology are encouraging, offering a range of possibilities for obtaining a variety of nanocomposite coatings with diverse chemical compositions, structures, and morphologies,[75] which is particularly interesting for us in terms of thin-film nanocatalysts. The essence of progress in this area is primarily related to the intensive development of APPD processes involving aerosols. The use of precursor solutions or nanoparticle dispersions in the form of an aerosol, similarly to the case of low-pressure PECVD discussed above, significantly broadens the range of components that can be used to build deposited films.[76]

Significant advances in the design of APPD reactors are also being observed. In addition to the most commonly used reactors, which operate on the basis of dielectric barrier discharge (DBD), increasing attention is being paid to plasma jet reactors (APPJ). They offer significantly greater flexibility in the deposition process than DBD, which requires flat and insulating substrates, thus eliminating the possibility of 3D deposition and the use of metal substrates.[77,78] It should be noted that the plasma generated in both APPJ and DBD reactors, similarly to low-pressure PECVD, is a cold (non-equilibrium) plasma.

To ensure deposition of films over large surfaces, moving substrates are introduced, for example using the roll-to-roll technique, which is much more difficult to apply in low-pressure reactors.[79] More sophisticated designs are also emerging, such as conducting deposition of SiO_2 on a moving substrate in the reaction zone between the gaseous organosilicon precursor and oxygen plasma introduced into this zone independently of each other.[80]

It is expected that further inventions in the field of APPD will fully realize the possibility of producing thin films of nanocomposites on various substrates, also structural materials, meeting the requirements for nanocatalysts for thermal processes.

3.3. Plasma-enhanced atomic layer deposition (PEALD)

When searching for the most precise thin-film deposition methods for molecular designs, the atomic layer deposition (ALD) method,[81] which often uses cold plasma in its technology (PEALD),[82,83] cannot be overlooked. In conventional temporal ALD, the substrate is cyclically exposed to alternating precursor and co-reactant, with purge steps for removing any unreacted precursors and by-products after each process. The use of plasma as a co-reactant effectively reduces heat demand and often allows for better film properties compared to films deposited by thermal ALD. Nevertheless, both ALD and PEALD have the main limitations of very low deposition rates and a cumbersome control system for multiple sequential process steps, which generally favors the PECVD method for practical applications.[84] However, this does not prevent large-scale research into the atomically precise design and synthesis of thin-film catalytic materials using ALD, including PEALD.[85]

An attractive approach to increasing both the deposition rate and the surface area of coated substrates is a modification of ALD known as spatial ALD. When cold plasma is used as the co-reactant, it is referred to as spatial PEALD. This involves separating the dosing of the precursor and co-reactant in space rather than time. Their streams are now continuously delivered to a reciprocating or rotating substrate, and time-consuming chamber purging steps are no longer necessary because inert gas shields separate the precursor streams between and around the reaction zones. These shields act as gas bearings, allowing for virtually frictionless movement between the reactor head and the substrate.[84,86,87] This solution also eliminates the need for low pressure, and the process can be conducted at atmospheric pressure.[84,88] A diagram illustrating the spatial PEALD concept and a schematic of an example wafer lab-scale rotating reactor are shown in Fig. 2f.

The visible progress in the development of ALD methods towards PEALD and spatial PEALD allows us to realistically look at their competitiveness with PECVD from a technological point of view. However, it should be remembered that the range of possible precursors, due to the specificity of ALD, is much narrower than that in PECVD. In the case of ALD, in addition to volatility, they must also be characterized by self-limiting surface reactions, resulting in the formation of only one monomolecular precursor layer on such a surface in each subsequent cycle.[81] Furthermore, despite the significant increase in the film deposition rate in spatial PEALD compared to that in typical temporal PEALD, it is still much slower than that in PECVD.[84] On the other hand, a significant advantage of PEALD (temporal and spatial) methods is excellent atomic-scale control of thickness and chemical structure. However, obtaining nanocomposite films composed of nanoparticles placed in a matrix in this way is a much more complicated task than using PECVD.[89] Among the advantages of PEALD, and temporal PEALD in particular, one should also mention the possibility of obtaining good uniformity and conformality over 3D substrates,[88,90] which is particularly important if we are considering the deposition of thin catalytic films on supports for structured reactors.

3.4. Deposition on 3D substrates

The essence of the concept of using cold plasma deposition methods to produce nanocomposites for thermocatalysis applications is their thin-film nature. This fundamental characteristic underlies new designs for packings for structured catalytic reactors, where the key challenge is the appropriate shape of the support, not the form of the catalyst, which, due to its thin-film nature, can be applied to any surface without changing the geometry of the packing. A reliable but highly limited solution for such designs is to manufacture the packing from a material that itself acts as a catalyst. For example, platinum and platinum–rhodium catalytic meshes have been in use for over a hundred years, but these are associated with very high operating costs.[91] Recently, attention has turned to 3D printing, which offers significantly greater possibilities due to its relatively low price and the ability to produce packings of virtually any shape. By adding a catalyst precursor directly to the robocasting ink, it is possible to obtain a packing with a designed shape and catalytic properties.[92,93] However, it is

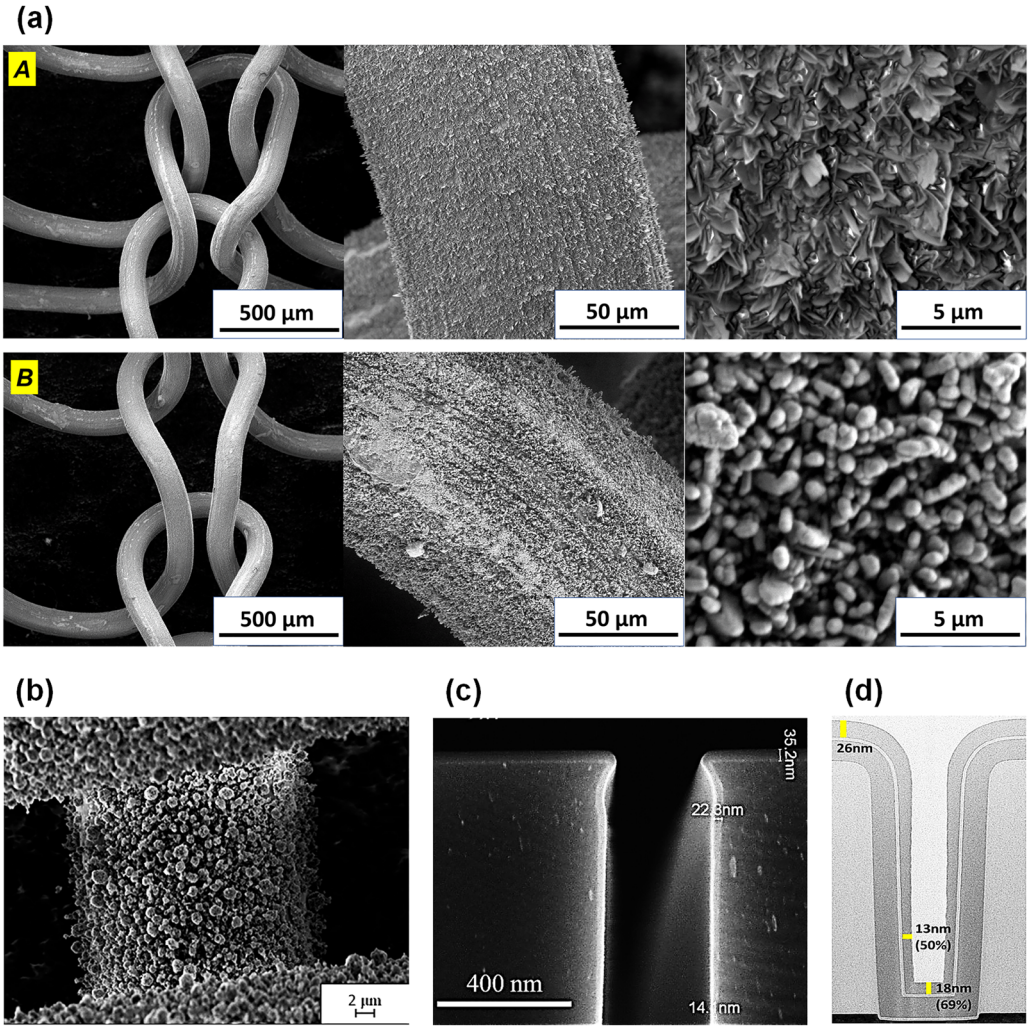

Fig. 3 Thin films deposited by cold plasma methods on 3D structures: (a) SEM images of a CoO_x-based nanocatalyst deposited by PECVD on a kanthal mesh: (A) – before deposition; (B) – after deposition, reproduced from ref. 26 with permission from Elsevier, copyright 2019. (b) SEM image of a nanocatalyst composed of TiO_2 nanoparticles and a silicon–carbon-oxide matrix deposited by APPD on a very dense mesh.[102] (c) SEM image of an SiN_x film deposited by PEALD in a 350 nm-wide trench structure, reproduced from ref. 103 with permission from AIP Publishing, copyright 2016. (d) Cross-sectional TEM image of an SiN_x film deposited by PEALD in a 100 nm-wide trench structure, reproduced from ref. 90 with permission from American Chemical Society, copyright 2017.

important to realize that the range of catalytic fillings that can be obtained in this way is quite narrow. It is therefore not surprising that attention is focused on thin-film coatings, among which cold plasma-deposited films are at the forefront.

Fig. 3a shows SEM images of a structured packing in the form of a kanthal mesh with a film produced by PECVD from a cobalt-organic precursor. Depending on the post-treatment of the deposited film, nanocomposites consisting of a carbon matrix and CoO or Co_3O_4 nanoparticles can be obtained (Section 4), which exhibit significant catalytic activity in CO_2 hydrogenation and hydrocarbon combustion, respectively.[21,26] Such films were also deposited in the same manner on kanthal plates,[51,94] from which, for example, structured channel packings can be constructed.[96] In addition to the CoO_x-based catalytic films, other nanocomposites, such as those containing CuO_x,[94,95] NiO_x,[97] FeO_x[98] nanoparticles, or more sophisticated nanohybrid structures, *e.g.*, CoO_x/CuO_x,[94,95] FeO_x/CoO,[99] and CoO/WO_3,[100] have been deposited by PECVD on the above-mentioned structured packing elements and successfully tested in thermocatalytic reactions. It should be emphasized that nanohybrid structures have recently attracted particular attention due to the observed formation of specific nanoscale heterojunctions, which determine the course of the catalytic process (more on this topic is written in Sections 4 and 5).

As can be seen, PECVD, in addition to its extensive capability to control the chemical composition and nanostructure of the produced films (Section 4), proves to be a good tool for depositing such films onto packing elements for structured reactors. Recently, even attempts have been made to use cold plasma, although only for surface treatment of 3D-printed structured elements,[101] but this is a clear indication that thin-film deposition using PECVD combined with 3D printing

will soon see the light of day. Proposals for research projects are already emerging that consider the technology of alternating the production of structured packing: 3D printing a fragment of the packing, deposition of a catalytic film on it using PECVD, then printing another fragment of the packing, and then depositing another film, until the entire complex packing structure is completed.

Of course, not only PECVD, but also other methods of thin film deposition using cold plasma, such as APPD (Section 3.2) or PEALD (Section 3.3), are being tested for their ability to coat supports of 3D topography. Fig. 3b shows, for example, a fragment of a very dense mesh covered with a film of a nanocomposite containing TiO_2 nanoparticles in a silicon–carbon-oxide matrix, deposited by APPD using an aerosol composed of a liquid mixture of hexamethyldisiloxane and isopropyl alcohol with a suspension of TiO_2 nanoparticles (10–50 nm) as a source of precursors.[102] Significant progress has also been recently observed in the use of PEALD for the deposition of thin films onto various 3D structures.[88] For example, 3D trench nanostructures were completely covered in this manner by depositing thin films of silicon nitride on their surfaces using volatile organic compounds containing silicon, or silicon and nitrogen atoms as precursors and nitrogen plasma as a co-reactant.[90,103] SEM images of such trench structures with a SiN_x film deposited are shown in Fig. 3c and d.

More spectacular attempts have also been made, for example, by PEALD producing a uniform thin film of ruthenium (15–60 nm thick) onto the surface of carbon nanotubes (30–40 nm in diameter and 13–15 μm long) forming a forest on a steel mesh. The three-dimensional structure of free-standing multi-walled carbon nanotubes allows for maximum utilization of the active material on their surface, which is crucial for catalytic processes.[104] Another example is the deposition of approximately 10 nm nickel nanoparticles onto the developed surface of cerium oxide (CeO_2), achieving excellent activity of this system in CO_2 methanation. Ni nanoparticles were produced by depositing nickel nitrate as a precursor on the CeO_2 surface, which was then decomposed using APPD in an argon atmosphere.[105]

When considering 3D structures, attention should also be paid to powder structures. Cold plasma deposition methods can be used to produce both supports and catalysts themselves in the form of powders. The production of powder structures by PECVD has been known and studied for a long time,[106,107] but only recently has there been a significant increase in interest in their applications as catalytic systems.[108]

Additionally, using cold plasma methods, thin-film catalytic structures can be deposited on powder supports. For example, Pd nanoparticles produced by the PEALD method and deposited on powder substrates consisting of a mixture of γ-Al_2O_3, amorphous aluminum silicate, and molecular sieve have been successfully used in the catalytic oxidation of CO. Palladium hexafluoroacetylacetonate was used as the precursor in this process, and hydrogen plasma as the co-reactant.[109] Recently, particular attention has been drawn to systems consisting of catalytic powder particles with a carbon nanolayer deposited on their surface, thus forming a core–shell or core–shell-like composite structure. At first glance, this may seem surprising, but these layers, in addition to increasing the stability of the core material, especially in transition metal catalysts, often also enhance catalytic activity. This effect may be related to the diffusion of reagents through the shell layer, which changes their residence time in contact with active sites, as well as to the formation of heterojunctions between the core and shell, which modify the active sites. However, these mechanisms, particularly in thermal catalysis processes that have already been tested for these systems, such as Fischer–Tropsch synthesis or hydrogenation reactions, are still undetermined and require further in-depth research.[110] It is worth noting that among the methods for producing carbon shell layers, PECVD is becoming increasingly attractive, typically using CH_4 as a precursor, leading to the deposition of graphene-like films.[111,112]

In summary, it is important to reiterate the wide range of possibilities offered by cold plasma deposition methods for forming thin films on 3D substrates, which currently represents a key challenge in the production of catalytic surfaces on structured reactor packings. It is also important to emphasize that the use of cold plasma for producing thin-film nanocatalysts on virtually any substrate (*e.g.*, thermosensitive materials such as polymers) and on substrates of any shape is becoming increasingly unrivaled.

4. Controlling the structure of deposited films

As discussed above, the production of thin films using cold plasma deposition methods offers extensive possibilities for designing and controlling their structure. This results from the vast array of precursors with diverse chemical structures and the wide range of parameters used for plasma deposition of films, as well as their possible post-treatments. The rational design and production of films with suitably tailored structures for a variety of applications are also increasingly being considered.[38,53,75,82,83]

Considering the topic relevant to us – plasma-deposited thin films with potential nanocatalytic properties suitable for thermocatalysis – we will limit further discussion of their structure to this class of materials.

As shown in Section 3.3, ALD is undoubtedly the most effective method for controlling the structure of the produced films, and its modification, PEALD, is particularly relevant here. However, as already mentioned, in terms of practical applications for thin-film nanocomposites, it still remains significantly inferior to direct plasma deposition methods such as PECVD or even APPD. Therefore, in our further discussion of controlling the molecular structure, nanostructure, and electronic structure of the films, we will focus primarily on these methods.

4.1. Molecular structure

From the perspective of potential heterocatalytic properties, the most interesting nanocomposites are those containing metal

nanoparticles or their combinations – primarily oxides, but also carbides, nitrides, sulfides, *etc*. The most common starting point for obtaining such films is the introduction of metal atoms during deposition. This is most easily achieved using appropriate volatile precursors, typically metal–organic complexes and, less frequently, inorganic metal compounds. Metal nanoparticles (or their oxides, for example) can also be introduced into the deposited film as preformed nano-objects in a hybrid PECVD + sputtering process, or by feeding such nano-objects into the PECVD reactor chamber in the form of an aerosol, although direct deposition from volatile precursors remains dominant (Section 3.1).

Table 1 lists examples of metal precursors used for plasma deposition of thin films with potential catalytic activity. Each serves as a source of the desired metal atoms, but if the goal is to obtain oxides, carbides, nitrides, *etc.* the corresponding elements must also be present in the plasma region. This can be achieved by incorporating them into the precursor structure or introducing them into the reaction mixture as separate chemical compounds. Often, the addition of an elemental gas is sufficient: for oxides – oxygen,[49] for nitrides – nitrogen,[114] for sulfides – sulfur vapor.[115] Volatile compounds of these elements are also used, most commonly NH_3, N_2H_4,[114] or H_2S.[116] It should also be noted that the carbon present in metal–organic complexes becomes a source of carbon structures in the resulting nanocomposite films, such as graphite-like carbon matrices[117] or carbon nanotubes.[98]

However, introducing the chemical elements needed to build the designed structure into the plasma is only the first step in such a process. The molecular structure of the film now depends on the conditions of the plasma process, which are influenced by many different factors, such as the type of deposition method (Section 3), reactor design, precursor feeding strategy, and process parameters (discharge frequency and power, partial pressures and flow rates of precursors, carrier gas type and its flow rate, substrate temperature, deposition time, *etc.*). Post-treatments – thermal,[117] plasma-based,[117] or laser-based[118] – may also play an important role. All these factors determine the chemical and physicochemical processes occurring in the plasma and on the substrate surface and then on the surface of growing film, ultimately defining its final molecular structure. Despite extensive knowledge of plasma chemistry, mechanisms of film formation, and many studies linking deposition to resulting molecular structures, no reliable algorithms and recipes yet exist for precisely designing a film by selecting specific deposition conditions.[38,119] Elements of ''alchemy'' are still present.

As an example of regulating the molecular structure of films by controlling the parameters of their deposition process in cold plasma, consider nanocomposites containing CoO and WO_3 oxides in a carbon matrix. These films were produced by co-deposition using $CpCo(CO)_2$ and $W(CO)_6$ as precursors, with the precursor mixture composition as the variable.

Table 1 Metallic precursors used for plasma deposition of thin films with potential catalytic properties. Liquid or solid precursors are introduced into reactors in a vaporized form *via* evaporation or sublimation, while liquid solutions are injected as aerosols

Metal precursor	Denotation	State under standard conditions	Introduced metal	Ref.
Platinum(II) acetylacetonate	$Pt(acac)_2$	Solid	Pt	
Palladium(II) acetylacetonate	$Pd(acac)_2$	Solid	Pd	
Palladium(II) hexafluoroacetylacetonate	$Pd(hfac)_2$	Solid	Pd	
Ruthenium(II) bis(ethylcyclopentadienyl)	$Ru(EtCp)_2$	Liquid	Ru	
Cobalt(III) acetylacetonate	$Co(acac)_3$	Solid	Co	
Cobalt(II) bis(2,2,6,6-tetramethyl-3,5-heptanedione)	$Co(TMHD)_2$; $Co(dpm)_2$	Solid	Co	
Cobalt(II) bis(cyclopentadienyl)	$CoCp_2$	Solid	Co	
Cobalt(I) cyclopentadienyldicarbonyl	$CpCo(CO)_2$	Liquid	Co	
Titanium(IV) tetraisopropoxide	TTIP	Liquid	Ti	
Titanium(IV) butoxide	TNBT; $Ti(OBu)_4$	Liquid	Ti	
Titanium(IV) ethoxide	$Ti(OEt)_4$	Liquid	Ti	21
Titanium(IV) diisopropoxidebis(2,2,6,6-tetramethyl-3,5-heptanedionate)	$Ti(O\text{-}i\text{-}Pr)_2(thd)_2$	Solid	Ti	
Zirconium(IV) acetylacetonate	$Zr(acac)_4$	Solid	Zr	
Zirconium(IV) tetra(*tert*-butoxide)	ZTB	Liquid	Zr	
Zirconium-*n*-propoxide	ZNP	Liquid	Zr	
Iron(III) acetylacetonate	$Fe(acac)_3$	Solid	Fe	
Iron(II) bis(hexafluoroacetylacetonate)-(*N*,*N*,*N*′,*N*′-tetramethylenediamine)	$Fe(hfa)_2$TMEDA	Solid	Fe	
Tert-butylferrocene	TBF	Liquid	Fe	
Iron(0) pentacarbonyl	$Fe(CO)_5$	Liquid	Fe	
Copper(II) acetylacetonate	$Cu(acac)_2$	Solid	Cu	
Chromium(III) acetylacetonate	$Cr(acac)_3$	Solid	Cr	
Nickel(0) tetracarbonyl	$Ni(CO)_4$	Liquid	Ni	97
Tungsten(0) hexacarbonyl	$W(CO)_6$	Solid	W	59
Copper(I) hexafluoroacetylacetonate - vinyltrimethylsilane	(hfac)copperVTMS	Liquid	Cu	58
η4-2,3-dimethylbutadiene ruthenium(0) tricarbonyl	$Ru(DMBD)(CO)_3$	Liquid	Ru	104
Titanium tetrachloride	$TiCl_4$	Liquid	Ti	113
Molybdenum pentachloride	$MoCl_5$	Solid	Mo	115
Cobalt nitrate dissolved in water	$Co(NO_3)_2/H_2O$	Liquid solution	Co	67
Dicobalt octacarbonyl dissolved in hexane	$Co_2(CO)_8/C_6H_{14}$	Liquid solution	Co	68

The elemental composition and molecular-level information were provided by X-ray photoelectron spectroscopy (XPS).[59] Fig. 4a shows the atomic content of W and Co obtained in this way, expressed as the W/(Co + W) ratio, and the carbon content in relation to the metal content (C/(Co + W)), presented as functions of precursor partial pressures ($PW(CO)_6/(PCpCo(CO)_2 + PW(CO)_6$). In turn, Fig. 4b shows the dependence of elemental composition on the W/(Co + W) ratio. These results confirm a well-known observation:[120,121] the elemental composition of the film does not match the composition of the reaction mixture. Establishing the precise relationship between these compositions – the basis for designing a specific molecular

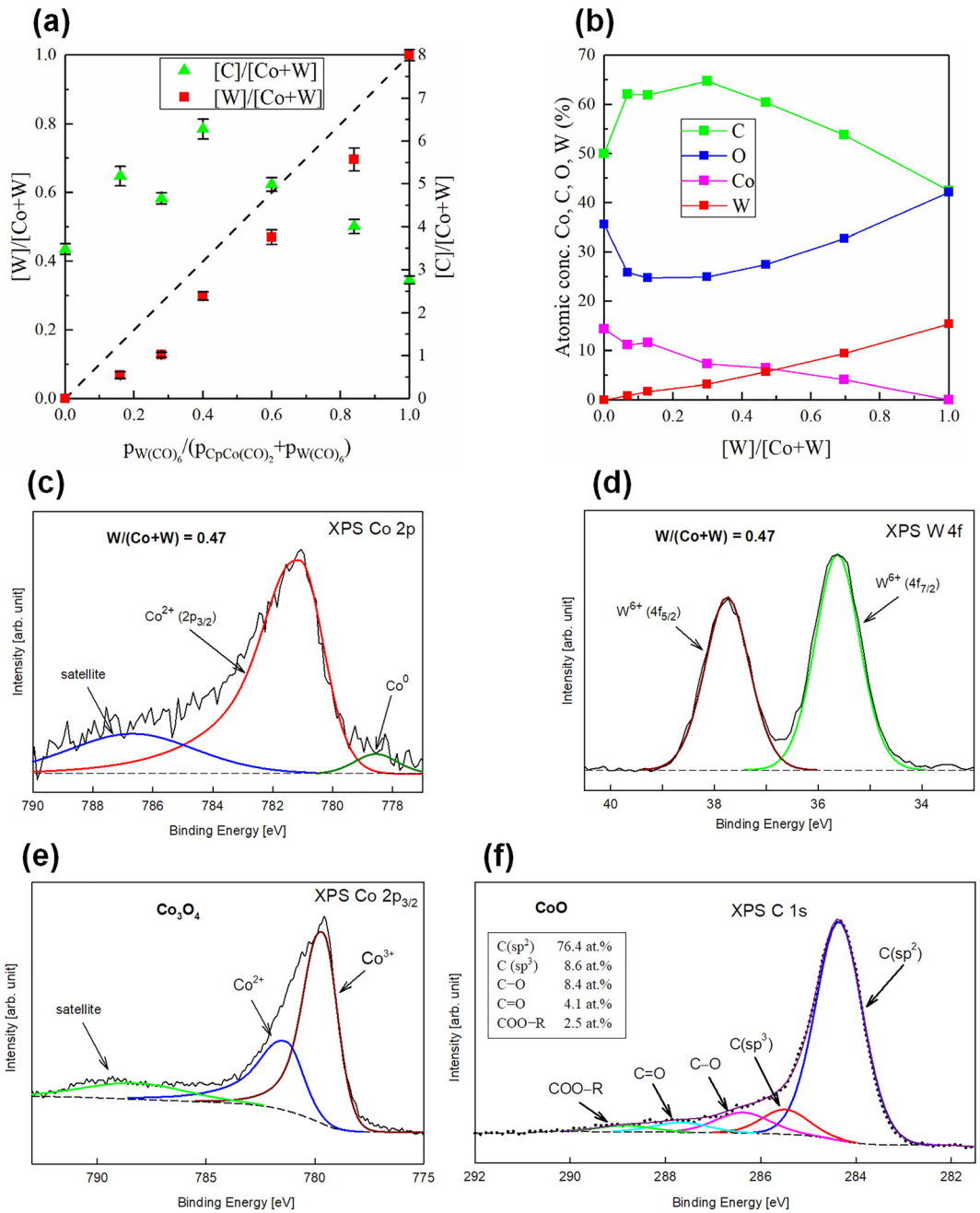

Fig. 4 Molecular structure of thin-film nanocatalysts deposited by PECVD: (a) atomic contents of cobalt, tungsten, and carbon, expressed as W/(Co + W) and (C/(Co + W)) ratios, as a function of precursor partial pressures for films co-deposited from $CpCo(CO)_2$ and $W(CO)_6$.[59] (b) Dependence of the overall elemental composition of the films in (a) on the W/(Co + W) ratio.[59] (c) and (d) XPS spectra of cobalt (Co 2p) and tungsten (W 4f), respectively, for a film with W/(Co + W) = 0.47 co-deposited from $CpCo(CO)_2$ and $W(CO)_6$, reproduced from ref. 100 with permission from Wiley-VCH, copyright 2025. (e) XPS spectrum of cobalt (Co 2p) for a film deposited from $CpCo(CO)_2$ followed by thermal treatment in oxygen.[118] (f) XPS spectrum of carbon (C 1s) for an example carbon matrix formed during plasma deposition from metal–organic precursors, reproduced from ref. 122 with permission from Elsevier, copyright 2019.

structure – requires, however, a deeper understanding of the complex film-formation mechanisms, which is still incomplete and demands further intensive research. Nevertheless, in this individual case, the desired film composition can be obtained by selecting an appropriate precursor ratio.

More detailed XPS studies provide deeper insight into the molecular structure of the films, offering further opportunities for tailoring the material. Fig. 4c and d show the XPS spectra of cobalt (Co 2p band) and tungsten (W 4f band), confirming CoO and WO_3 formation. By varying the ratio of precursors in the reaction mixture, as shown in Fig. 4a, the CoO and WO_3 contents can be controlled in the deposited films.[100]

In addition to controlling the parameters of the plasma deposition process, the molecular structure of the films can also be tailored through post-treatment of such films. An example would be films produced, similarly to those above, from a cobalt precursor ($CpCo(CO)_2$) and then subjected to short thermal treatment (623 K, 15 min is sufficient) in an argon or oxygen (air) atmosphere.[26,122] In the former case, nanoparticles of CoO are present in the film, as evidenced by the XPS spectrum similar to that shown in Fig. 4c. However, after thermal treatment in oxygen, the film contains nanoparticles of cobalt spinel Co_3O_4, as confirmed by the XPS spectrum (Fig. 4e). Thus, short thermal treatment of the deposited film in a suitable atmosphere can dramatically alter the catalytically active phase, making post-treatment an additional tool for rational control of molecular structure of films deposited by cold plasma.

When fabricating thin films from metal–organic precursors, it is important, as mentioned earlier, to account for the presence of carbon, which – as a result of plasma processes – typically forms the matrix of the deposited nanocomposite. Depending on the deposition conditions, the molecular structure of this matrix can vary and, as will be shown later (Section 4.3), may influence the catalytic properties of the nanocomposite.[117] Fig. 4f shows a typical XPS C 1s spectrum of the above-discussed film post-treated thermally in argon.[122] A very high content of sp^2 carbon relative to sp^3 carbon can be seen here, which indicates a graphite-like matrix structure. A small amount of oxygen bound to the matrix in the form of various functional groups is also visible.

As in the case of metal-based fractions, we also have certain possibilities to control the structure of the carbon matrix. For example, when conducting the PECVD process in a precursor-deficient region, the elemental composition of the film produced from the $CpCo(CO)_2$ precursor remains virtually unchanged as a function of glow discharge power.[118] However, an increase in power, and thus an increase in self-bias potential, causes an increase in the energy of the ions bombarding the growing film. This effect can also be achieved by applying a controlled bias directly to the electrode on which the film is deposited. The increase in the energy of ion bombardment of the growing carbon matrix leads to an increase in the number of carbon atoms in sp^3 hybridization at the expense of sp^2 and a structural transition from graphite-like to diamond-like.[123] Thus, discharge power can be used to modify the molecular structure of the carbon matrix. Similarly, flow rate, pressure, and substrate temperature,[124,125] as well as thermal post-treatment,[117] can be employed.

As can be seen, we have a wide range of process parameters at our disposal, the selection of which allows us to influence the molecular structure of the deposited films. However, despite significant recent progress and emerging attempts to model plasma deposition processes,[126–128] the traditional ''trial and error'' approach is still often necessary to obtain the designed molecular structure.

4.2. Nanostructure

When considering nanocomposites for catalysis, nanoparticles are undoubtedly the key nanostructural elements responsible for catalytic behavior.[7,129] Using cold plasma deposition methods to produce nanocomposites, the first quite obvious way to obtain their structure in the form of a matrix containing nanoparticles with a predetermined chemical composition, size, and condensation seems to be the hybrid PECVD + sputtering method (Section 3.1). By adjusting deposition parameters, target composition, and reaction mixture composition, one can strive to produce films with a precisely defined nanostructure. However, this challenge is not trivial, because the complex and competing mechanisms of nanocomposite formation complicate the establishment of a simple correlation between deposition conditions and nanostructure.[62,130] Recent observations in this area, however, are bringing us closer to a more rational design of the deposition process toward the desired nanostructure.

One example is the deposition of nanocomposite films containing a silicon–carbon-oxide matrix and TiO_2 nanoparticles.[63] The reaction mixture (with an operating pressure of 4 Pa) consisted of hexamethyldisiloxane (20%), oxygen with a content of 0 to 50%, and argon varying from 80 to 30% to maintain a constant operating pressure during the experiments, and the target was titanium dioxide powder. By controlling the ratio of O_2 and Ar in the plasma, the composite nanostructure can be adjusted by changing the concentration, size, and form of the particulate phase. Fig. 5a and b shows the effect of oxygen content in the reaction mixture on TiO_2 agglomerate morphology.

Another example is the production of nanocomposites containing titanium carbide nanoparticles in an amorphous carbon matrix.[64] In this case, the size of TiC nanocrystallites formed by sputtering a Ti target in an acetylene and argon atmosphere at low pressure (approximately 1–2 Pa) was regulated. By changing the C_2H_2 flow rate, not only the carbon content in the deposited nanocomposite was controlled, but also the average size of the TiC nanocrystallites, as shown in Fig. 5c.

It was also shown that the size of nanoparticles is influenced by the deposition time.[131] When depositing a film of the nanocomposite consisting of a diamond-like matrix and silver nanoparticles, their average size was changed from 7 to 22 nm by extending the process time from 10 to 40 min.

Recent progress in hybrid PECVD + sputtering systems, unfortunately, does not eliminate all the shortcomings of

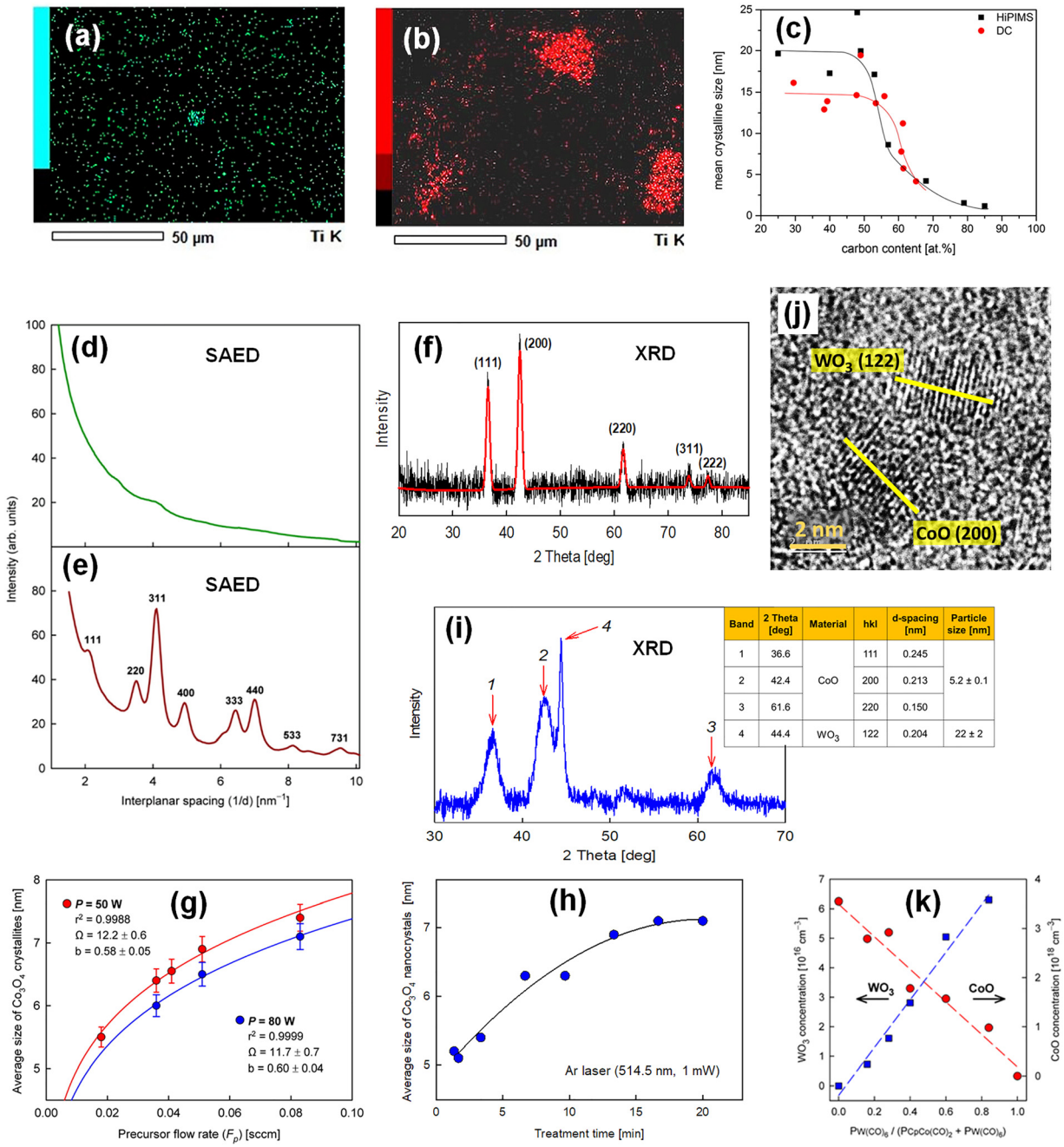

Fig. 5 Nanostructure of thin-film nanocomposites deposited by cold plasma methods: (a) and (b) Ti atomic intensity maps for films composed of TiO_2 nanoparticles embedded in a silicon–carbon-oxide matrix, deposited by a hybrid PECVD + sputtering method using a reaction mixture containing 20% and 50% oxygen, respectively.[63] (c) TiC nanocrystallite size as a function of carbon content in films deposited by a hybrid PECVD + sputtering method using a Ti target and varying acetylene content in a C_2H_2/Ar reaction mixture; two deposition modes – direct-current magnetron sputtering (DC) and high-power impulse magnetron sputtering (HiPIMS) – were applied, reproduced from ref. 64 with permission from Elsevier, copyright 2017. (d) and (e) Electron diffraction (SAED) patterns of CoO_x-based films fabricated by PECVD, as-deposited (amorphous structure) and after thermal treatment in oxygen (Co_3O_4 structure), respectively.[118] (f) XRD pattern of the same CoO_x-based film after thermal treatment in argon (CoO structure).[117] (g) Dependence of the Co_3O_4 nanocrystalline size on the $CpCo(CO)_2$ precursor flow rate and discharge power for films deposited by PECVD and subsequently thermally treated in oxygen; the curves represent a model describing the nucleation and growth of these nanocrystallites.[118] (h) Regulation of the Co_3O_4 nanocrystallite size using an argon laser to precisely control the thermal treatment time for films deposited analogously to those in (g), reproduced from ref. 26 with permission from Elsevier, copyright 2019. (i) XRD pattern of a nanocomposite film containing CoO and WO_3 nanoparticles in a carbon matrix fabricated by PECVD co-deposition, and (j) HRTEM micrograph revealing fragments of crystallographic planes that correspond to these nanoparticles, reproduced from ref. 100 with permission from Wiley-VCH, copyright 2025. (k) Concentrations of CoO and WO_3 nanoparticles as a function of precursor partial pressures for films co-deposited by PECVD using $CpCo(CO)_2$ and $W(CO)_6$; the plot is based on numerical data reported in ref. 100.

this method. The main disadvantages include difficulty of controlling nanoparticle aggregation and ensuring their uniform distribution within the matrix, which makes the properties of such nanocomposites, including their catalytic properties, less reproducible.[62,131] This issue is much less pronounced in PECVD alone. With metal–organic precursors, the nature of the film deposition mechanisms and chemical reactions taking place in the plasma determine the nanoparticle nucleation pathways and phase separation processes during film growth, which in an environment of initially atomic dispersion of metal atoms leads to significantly better control of the size and distribution of the resulting nanoparticles. In recent years, such nanocomposites have been successfully produced (Section 4.1) and tested in thermocatalysis (Section 5).

Let us return to the example of films produced by PECVD from a cobalt precursor ($CpCo(CO)_2$), mentioned in Section 4.1. Fig. 5d–f show the diffraction patterns of the deposited film and films subjected to short thermal treatment in air and argon atmospheres after deposition. As can be seen, the type of treatment dramatically changes the cobalt oxide phase – from amorphous to nanocrystalline Co_3O_4 or CoO, respectively.[117,118]

It has also been shown that the size of the formed nanocrystallites depends on deposition parameters, such as the precursor flow rate and discharge power. These relationships for Co_3O_4 spinel nanocrystallites are shown in Fig. 5g, where the experimental results largely correspond to the developed model describing the nucleation and formation of these nanocrystallites.[118] Furthermore, precise control of thermal treatment time – *e.g.*, *via* laser heating – allows tuning the nanocrystallite size (Fig. 5h).[26,118]

Nanocomposite films containing nanoparticles of two different semiconductors in the matrix are particularly important today due to their potential thermocatalytic applications. The molecular structure of such films produced by PECVD in co-deposition from $CpCo(CO)_2$ and $W(CO)_6$ precursors was discussed in Section 4.1. Now let us take a look at their nanostructure. Studies performed using X-ray diffraction (XRD) (Fig. 5i) and high-resolution transmission electron microscopy (HRTEM) (Fig. 5j) revealed the presence of CoO and WO_3 nanocrystallites with average sizes of 5.2 and 22 nm, respectively, in the films subjected to short thermal treatment in argon. In turn, molecular structure analysis (Section 4.1) enabled determining their concentration (Fig. 5k), interparticle distances, and the resulting mutual interactions expressed through nanoscale heterojunction formation, key determinants of catalytic activity.[100]

The ability to produce a thin nanocomposite film with an appropriate nanostructure is the guiding goal in the search for a rational design strategy for nanocatalysts dedicated to specific thermocatalytic processes. This pursuit is based on the close relationship between a material's nanostructure and its electronic structure, which ultimately governs its catalytic activity. All efforts aimed at controlling the molecular structure – and especially the nanostructure – are directed toward achieving the ability to precisely tune the electronic structure of the deposited film.

4.3. Electronic structure

It has long been known that the electronic structure of a material's surface determines its catalytic properties, or more precisely, the nature, type, and concentration of active sites governing the catalytic process, through a direct influence on the adsorption and activation of reactants at these sites.[132] Therefore, by controlling the electronic structure, we can control the course of catalytic reactions, their activity, and selectivity. It is now widely believed that without electronic effects closely related to the electronic structure of the surface, catalysis would not be possible.[133] Controlling the molecular structure and nanostructure is therefore primarily aimed at obtaining the appropriate electronic structure enabling the intended catalytic process to occur.

In recent years, particular attention has been paid to nanocomposites containing nanoscale heterojunctions – electronic junctions between two different materials, typically semiconductors. Two key aspects drive this interest: (I) the real possibility of controlling catalytic processes by designing appropriate heterojunctions, and (II) the practical feasibility of producing such heterojunctions using PECVD, which also enables their deposition as thin films suitable for constructing packings for structured reactors, as mentioned several times above.[134]

The essence of the nanoscale heterojunction concept is based on the assumption that the sizes of the nanoparticles forming these junctions are comparable to the depletion or accumulation region thicknesses. Under such conditions, entire nanoparticles may become filled with space charge (positive or negative), strongly modifying the nature of the catalytically active sites. Fig. 6a illustrates this principle for a model catalytic reaction A + B → C + D on nanoparticles of semiconductors S_1 and S_2. Formation of the heterojunction completely changes performance and selectivity compared with isolated nanoparticles.[134]

Heterojunctions between nanoparticles of different semiconductors are already widely used in photocatalysis – for example, in water splitting[135,136] and CO_2 photoreduction[137,138] – where the role of space charge is usually limited to creating an internal electric field that separates photogenerated electrons and holes, and the entire catalytic process occurs solely due to these carriers. On the other hand, a new approach to nanoscale heterojunctions and their application in thermocatalysis (without photogeneration) is based on the permanent modification of active sites induced by the presence of space charge. For example, a change in the nature of the active sites from acidic to basic, or *vice versa*, has been observed (Section 5). The possibility of controlling thermocatalytic processes through appropriate heterojunction design has been suggested for some time,[98,99,139] but convincing experimental evidence has only recently emerged.

Returning to PECVD co-deposited films from $CpCo(CO)_2$ and $W(CO)_6$ precursors (Section 4.2), strong evidence for CoO/WO_3 heterojunction formation was obtained.[100] The key result is the shift in XPS maxima for Co 2p and W 4f (Fig. 4c and d) as a function of composition. As shown in Fig. 6b and c, with increasing CoO content relative to WO_3, the analyzed XPS band

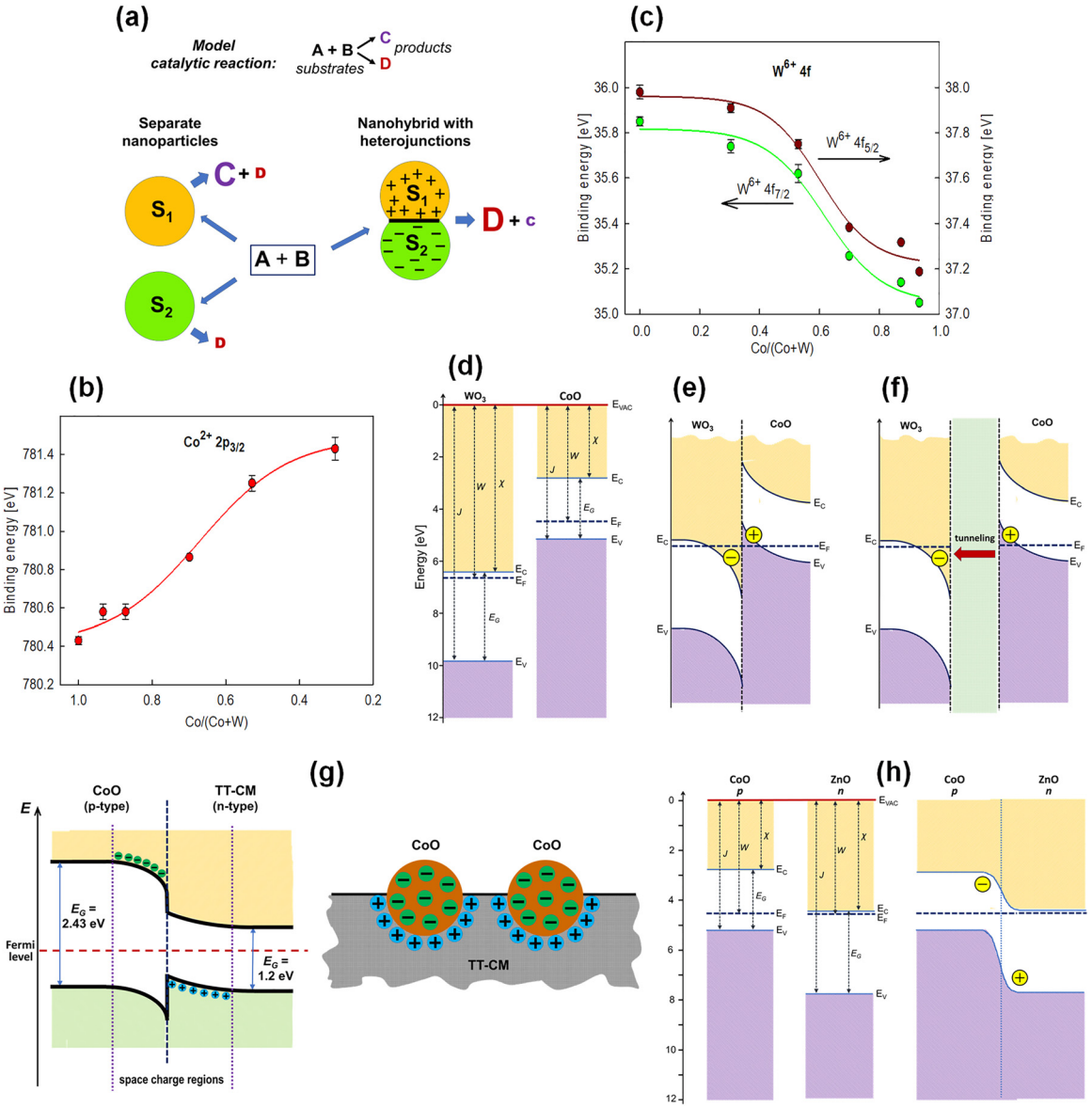

Fig. 6 Electronic structure of thin-film nanocatalysts deposited by PECVD: (a) schematic model illustrating the role of nanoscale heterojunctions in thermal catalysis. Nanoparticles of two different semiconductors (S_1 and S_2) form a heterojunction; the resulting space charge regions within the nanoparticles lead to pronounced changes in catalytic performance and selectivity for a model reaction compared with separately tested S_1 and S_2.[134] (b) and (c) Shifts of the Co 2p and W 4f XPS bands, respectively, as a function of Co and W contents in nanocomposite films containing CoO and WO_3 nanoparticles, co-deposited from $CpCo(CO)_2$ and $W(CO)_6$, reproduced from ref. 100 with permission from Wiley-VCH, copyright 2025. (d)–(f) Band-diagram models of WO_3 and CoO for (d) isolated nanoparticles, (e) a heterojunction formed by direct contact between the nanoparticles, and (f) a heterojunction with the nanoparticles separated by a distance not exceeding the maximum tunneling length, reproduced from ref. 100 with permission from Wiley-VCH, copyright 2025. (g) Band-diagram model of a heterojunction between a CoO nanoparticle and a carbon matrix (TT-CM) for a CoO_x-based film thermally treated in argon after deposition; a schematic representation of the nanocomposite surface with heterojunctions is also shown.[117] (h) Hypothetical CoO/ZnO heterojunction, yet to be realized, predicted to induce negative charge on CoO and thereby enhance CO_2-to-CH_4 conversion, reproduced from ref. 100 with permission from Wiley-VCH, copyright 2025.

for cobalt shifts toward higher binding energies, while the band for tungsten shifts toward lower energies. This effect is interpreted as the appearance of positive charges on CoO and negative charges on WO_3, which results from the formation of a CoO/WO_3 heterojunction. A closer analysis of the electronic structure of this heterojunction revealed that it is of type III (broken-gap). Furthermore, it was determined that its formation does not require an atomically sharp interface between the nanoparticles, but it is enough that they are located at a distance of no more than 10 nm from each other, and the interaction between them resulting from electron tunneling ensures the formation of the heterojunction. Fig. 6d–f show the band model for isolated CoO and WO_3 nanoparticles and for the formed heterojunction both in direct

contact and with the participation of the electron tunneling mechanism.

Nanoscale heterojunctions can also be created in a nanocomposite between semiconductor nanoparticles and a matrix that is characterized by a specific electronic structure.

An example of such a solution is a nanocomposite deposited by PECVD from a $CpCo(CO)_2$ precursor and subjected to a short thermal treatment in argon, composed of a carbon matrix with CoO nanoparticles.[117] The band model of this junction, the formation of which is confirmed by a shift in the XPS band for Co 2p toward lower binding energies compared to the film before thermal treatment, in which such heterojunctions do not form, is presented in Fig. 6g. This figure also shows a graphical model of the nanocomposite surface with the presence of heterojunctions. The resulting negative charge on the CoO nanoparticles enhances the basic nature of active states and increases catalytic activity toward methane formation in CO_2 hydrogenation (Section 5.2).

The examples above highlight the crucial role of nanoscale heterojunctions in controlling thermocatalysis and raise justified expectations for their broader use, especially given that cold plasma deposition provides an excellent tool for producing such systems. Initial efforts toward designing catalytic heterojunction systems are already under way. Fig. 6h shows a hypothetical CoO/ZnO heterojunction that would result in negative charge on CoO and thereby enhance CO_2-to-CH_4 conversion.[100] The use of PECVD for co-deposition from metal–organic precursors of cobalt and zinc is likely to make such a system feasible.

5. Plasma-deposited thin-film nanocomposites in thermocatalytic practice

Building on the strategies of controlling the structure of deposited films discussed in Section 4, the following section illustrates how these thin-film nanocomposites perform in practical thermocatalytic systems. Two factors motivate their development: the shift from particulate catalysts to thin-film forms that offer better integration with the reactor, and the trend of replacing noble-metal catalysts by non-noble alternatives that provide comparable performance at lower cost. Among the tested nanocomposites, cobalt–based nanomaterials have been extensively investigated due to multiple oxidation states and nanostructures of CoO_x, as already reported in Section 4, which enable catalytic versatility in various processes. Specifically, plasma-deposited CoO- and Co_3O_4-based thin films have shown promising catalytic performance in hydrocarbon oxidation,[49–52,98,140] CO_2 hydrogenation[97–99,117,122,141,142] and liquid-phase processes such as CO_2 hydration[143,144] and pollutant ozonation.[145,146] Their widespread use has provided valuable insight into how composition and nanostructure govern catalytic behavior, supporting the rational design of catalytic functions. From an engineering perspective, the thin-film form offers unique advantages: these catalysts can be precisely tailored by depositing them onto different 3D supports suited for specific reactor configurations. This approach, combined with the ability to control the nanocomposite structure through the parameters of plasma deposition, facilitates efficient thermocatalytic applications.

5.1. Oxidation reactions

As noted in Section 2, the pioneering use of PECVD in this field involved the fabrication of thin-film catalysts containing nanocrystalline Co_3O_4 spinel embedded in a carbon matrix on metallic 3D supports (such as chromium–aluminum steel meshes and sheets), which exhibited high activity in *n*-hexane combustion.[49,50] Subsequent studies by the same research group showed that under carefully adjusted plasma conditions, including oxygen in the reactive gas phase and appropriate discharge power, films containing highly dispersed Co_3O_4 spinel nanostructures could be obtained without the need for post-deposition calcination,[51] as was required in the earlier work.[49]

The plasma-deposited Co_3O_4 films exhibited higher low-temperature activity in *n*-hexane oxidation than conventional PtRh wire-gauze catalysts and Co foil oxidized to Co_3O_4.[51] These films also showed comparable catalytic activity to a commercial Pt/Al_2O_3 catalyst. The superior performance of the plasma-deposited Co_3O_4 films was attributed to two main factors. First, it was linked to improved mass-transport properties resulting from the use of wire gauze as a support, allowing better access of reactants to active sites compared to traditional porous carriers and flat sheets. Secondly, there is no doubt that the composite nanostructure plays a crucial role: $\approx$ 5 nm-sized nanocrystalline Co_3O_4 particles embedded in a carbon matrix showed higher activity compared to Co_3O_4 catalysts formed by oxidation of Co foil, which lack the carbon component, despite the higher loading of cobalt oxide in the latter.

A meaningful comparison of the performance of plasma-deposited Co_3O_4 nanocomposites with a reference Co foil oxidized to Co_3O_4 was obtained from reaction-rate measurements of n-hexane combustion performed in the temperature range of 100–550 °C.[140] These kinetic experiments, carried out in a continuous gradientless flow reactor, provided the apparent reaction rate (mol m^{-2} s^{-1}) expressed per external geometric surface area of the catalyst, as presented in Fig. 7a. The rates were determined for Co_3O_4 films deposited on wire mesh and flat metallic sheets, and numbers in parentheses indicate different deposition times, corresponding to different catalyst thicknesses. The results show that catalysts deposited on wire meshes exhibit substantially higher performance than those deposited on flat sheets, and both outperform the oxidized Co foil. This order clearly demonstrates the strong influence of structured supports and the specific nanostructure of the films on apparent catalytic activity.

Also from the practical implementation perspective, the PECVD films exhibited high dispersion, strong adhesion to the metallic microstructures, and controlled thickness, while maintaining the original geometry of the support. Moreover, compared to Langmuir–Blodgett (LB) film deposition or wet

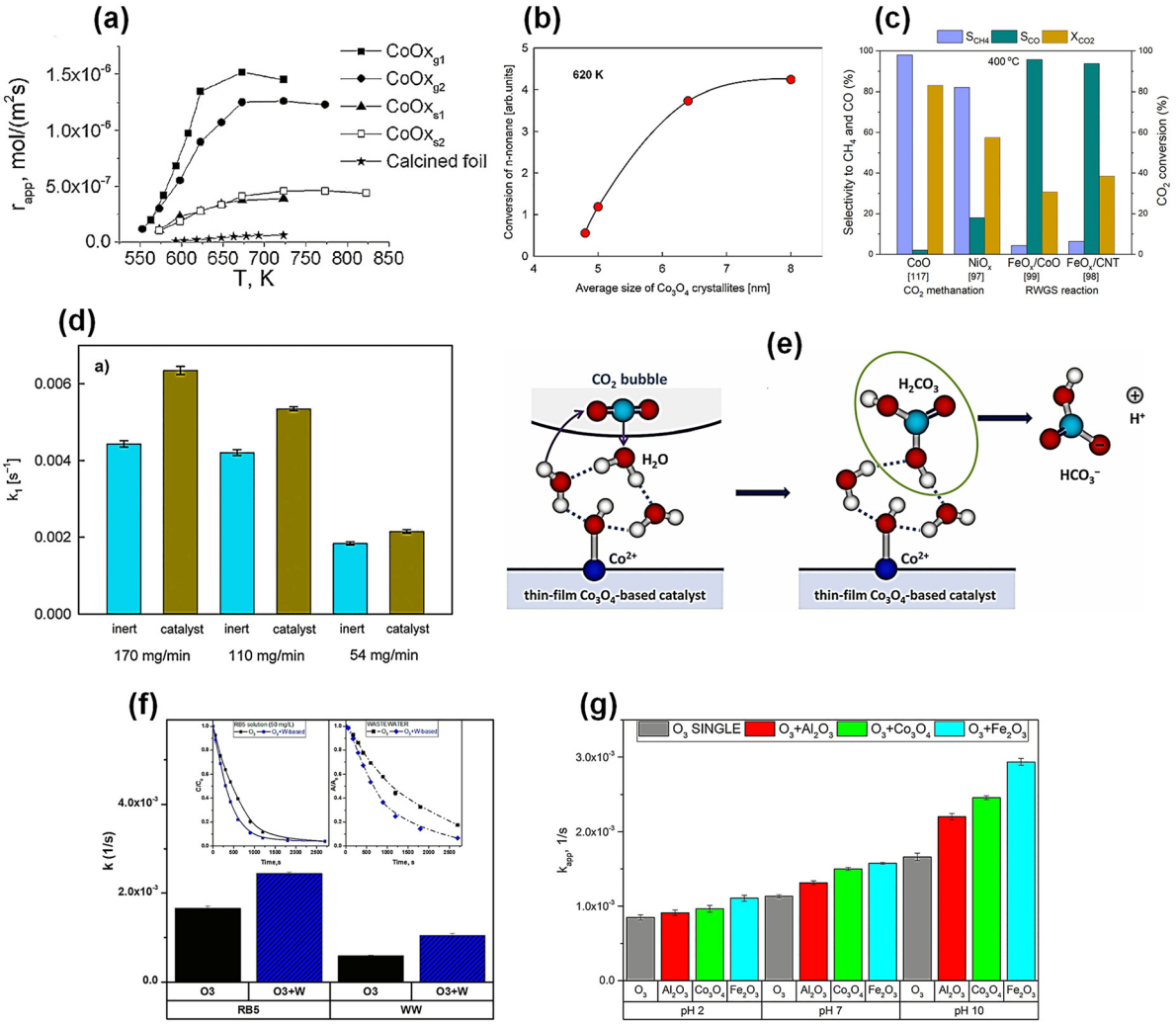

Fig. 7 Catalytic performance of plasma-deposited thin-film nanocomposites in various reactions. (a) Apparent reaction rate γ_{app} of n-hexane combustion for plasma-deposited Co_3O_4 films on wire-gauze, g, and flat-sheet, s, supports, compared with Co foil oxidized to CoO_x (Co_3O_4). Numbers in the subscript correspond to different catalyst thicknesses, adapted from ref. 140 with permission from Elsevier, copyright 2017 (b) Relative n-nonane conversion as a function of the Co_3O_4 nanocrystallite size, demonstrating that the controlled nanostructure tailored by deposition parameters directly enhances the catalytic performance of thin-film nanocomposites in catalytic combustion.[118] (c) Comparative performance of the best plasma-prepared thin film nanocomposites tested in CO_2 methanation and RWGS reaction under the same experimental conditions at 400 °C. Based on data reported in several studies.[97–99,117] (d) Average water-side mass transfer rate coefficients for CO_2 hydration at different flow rates for inert and plasma-deposited Co_3O_4 meshes.[144] (e) Scheme of CO_2 hydration catalyzed by a plasma-deposited Co_3O_4 thin film.[143] (f) Comparison of kinetics of single and catalytic ozonation over the best W-based thin-film composite for RB5 decomposition (simulated wastewater) and industrial textile wastewater (WW). The notation O_3 + W indicates ozonation performed in the presence of a W-based catalyst.[145] (g) Catalytic activity of Co_3O_4- and Fe_2O_3-based thin-film composites expressed as the apparent rate constant (k_{app}) for dye decolorization at different pH values. Data referring to Al_2O_3 correspond to a mesh coated with an Al_2O_3 layer developed by calcination of the kanthal support.[146]

impregnation, PECVD offered better control over catalyst dispersion and surface coverage.[51] Due to the high surface area and efficient utilization of the catalyst under different flow regimes, enabled by the gauze carriers, this kind of catalyst allows for a much more compact reactor compared to standard monolithic converters. The concept was then verified in a prototype large-scale structured reactor built from stacked catalytic knitted wire gauzes (Fig. 8a).[52] This validation confirmed the significant advantages of cold-plasma deposition for producing efficient thin-film catalysts and demonstrated clear benefits for designing compact and efficient catalytic reactors for VOC abatement.

Based on the encouraging results related to single oxide (Co_3O_4) thin film catalysts, another approach demonstrated that copper doping, achieved through a co-deposition technique using both copper and cobalt precursors in a single plasma deposition process, enhances the activity of cobalt oxide catalysts.[94] The resulting mixed Co/Cu oxide nanocomposite was also deposited on wire meshes and exhibited a higher nhexane combustion rate and lower reaction initiation temperature ($\approx$ 220 °C) compared to single Co_3O_4 thin-film catalysts, which ignited at around 280 °C. As can be seen, these results are clear evidence of a synergistic effect arising from the

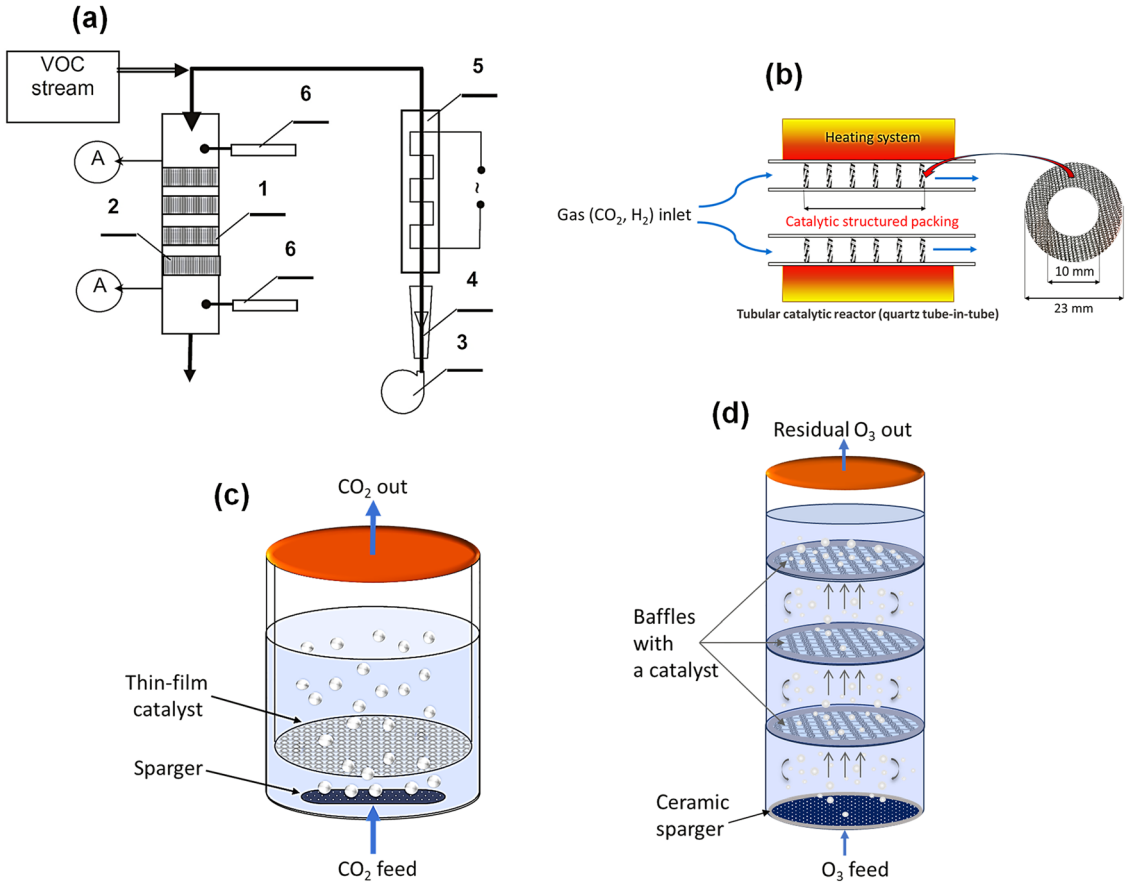

Fig. 8 Examples of structured catalytic reactor designs for gas-phase and multiphase reactions. (a) Prototype of a large-scale structured reactor used for VOC oxidation: (A) analysis probes. 1 – reactor; 2 – sheets of the catalytic gauze; 3 – blower; 4 – flow meter; 5 – electric heater; 6 – thermocouple, reproduced from ref. 52 with permission from Elsevier, copyright 2012. (b) The design of the small-scale tube-in-tube catalytic structured reactor used for testing the performance of CO_2 hydrogenation over thin-film catalysts.[143] (c) Lab-scale catalytic bubble reactor equipped with plasma-deposited thin films on wire mesh for testing CO_2 hydration in water.[143] (d) Pilot-scale catalytic bubble reactor incorporating baffles and wire mesh sheets coated with thin films for wastewater ozonation (based on patent claim EP23215146.4).[143]

combination of the two metal oxides in the nanocomposite. The application of plasma-deposited Co_3O_4 films was successfully extended to oxidation of methane[140] and nnonane.[118] The latter work highlighted a key advantage of cold-plasma deposition: its ability to precisely tailor Co_3O_4 nanocrystalline size, through controlled process parameters, as detailed in Section 4.2. A particularly practical finding was that increasing the flow rate of the cobalt precursor during PECVD leads to larger Co_3O_4 nanocrystallites in the resulting films, providing a useful strategy for the controllable nanocomposite design. This tuning of the nanostructure directly impacts the performance – n-nonane conversion increases with the nanocrystallite size. Fig. 7b illustrates this trend, showing how relative conversion efficiency improves with increasing size of Co_3O_4 nanocrystallites in the plasma-deposited films.

The high activity and stability of plasma-deposited Co_3O_4 thin films in the combustion of various harmful compounds, including n-hexane, n-nonane, and methane, together with the ability to precisely tailor their nanostructure, represent a significant advancement in the fabrication of thin-film nanocomposites by PECVD for catalytic processes.

The oxidation of CO represents another thermocatalytic reaction where plasma-deposited Co_3O_4 thin films have shown remarkable performance.[68] The approach used to prepare these films, based on the decomposition of a liquid precursor solution in plasma, was already discussed in Section 3.1. The films were applied to the walls of the microchannels of a microreactor. The use of cold plasma was particularly beneficial in this case, as the polydimethylsiloxane (PDMS) walls could otherwise melt if conventional methods of catalyst coating were applied. The authors demonstrated that the parameters of plasma deposition and post-treatment significantly influenced the crystalline properties of Co_3O_4 and consequently, its catalytic activity. Crystalline nano-sized Co_3O_4 exhibited excellent catalytic performance in CO oxidation, achieving nearly complete conversion and long-term stability, while amorphous Co_3O_4 led to a much lower conversion (42%). The study highlighted that the plasma method for applying catalytic films onto thermally sensitive microreactor wall materials is highly advantageous for preserving material integrity and ensuring high activity.

Expanding the above concepts, cold plasma-deposition methods have also been effectively applied to structured

supports such as metallic foams.[147] In these systems, plasma deposition was used to create an intermediate primer layer: a polysiloxane-based film, which acts as a protective interlayer for the subsequently introduced VO_x/TiO_2 catalyst. This plasma-deposited primer prevents oxidation of the substrate, and thereby enables selective oxidative dehydrogenation of propane, increasing propene selectivity by about 10% at any given conversion when compared with unprotected foams. However, the subsequent catalyst fabrication steps, including dip-coating TiO_2 and grafting polyvanadate species, were fabricated by conventional methods rather than PECVD. Nevertheless, this example illustrates the additional, useful role of plasma deposition in the fabrication of protective films on the complex structured supports.

Despite the advantages of cold plasma methods for depositing thin films on structured packing supports, these techniques are also highly effective for preparing catalysts on powder supports, as discussed in Section 3.4. For instance, metallic Pd nanoparticles were uniformly deposited by a PEALD process on alumina-based powder supports, with precise control over Pd loading and average nanoparticle size.[109] This tunability resulted in catalysts with excellent CO oxidation performance, achieving complete conversion at 140 °C under a gas hourly space velocity of 24 000 h^{-1} for an optimal Pd loading of $\approx$ 2 wt% and an average particle size of 2.9 nm.

5.2. CO_2 hydrogenation to CH_4 and CO

In recent years, several nanocomposites based on CoO_x, FeO_x, and NiO_x have been prepared by PECVD, characterized, and tested for CO_2 hydrogenation to methane and CO.[97–99,117,122,141,142] The performance of these catalysts was mainly evaluated in a small-scale tube-in-tube structured reactor (Fig. 8b). Among listed metal oxides, plasma-deposited thin-film catalysts based on cobalt oxide have shown particularly promising performance in CO_2 methanation,[117,122,140,141] which is a highly demanding reaction in terms of heat management because it is strongly exothermic. This introduces significant operational challenges in conventional packed-bed reactors, where uneven heat distribution often leads to local hot spots, catalyst deactivation, and reduced process efficiency. Thin-film catalysts deposited on structured metallic supports effectively address these operational issues due to the conductive nature and special geometry of the metallic support which ensures efficient heat transfer and mechanical stability. In addition, the structured mesh support provides high surface area for plasma deposition of nanostructured catalytic films.

Fundamental research in this area is focused on understanding how the chemical structure and nanostructure of cobalt-based films govern their catalytic performance.[117,122,141] The important finding is that CoO is responsible for the very high activity in CO_2 methanation, not metallic Co as commonly reported.[122] The most effective CoO nanocomposite, among the prepared films, consists of nanocrystalline CoO ($\approx$ 10 nm) embedded in a carbon matrix, forming a nanoscale p–n heterojunction.[117] As discussed in detail in Section 4.3, these electronic effects can strongly enhance adsorption and activation of reactant molecules, resulting in superior catalytic performance. This important finding aligns with the concept that acidic sites (positively charged) suppress CH_4 formation, whereas basic sites (negatively charged) promote it.[148,149] As a result, plasma-deposited CoO-based thin films achieved $X_{CO_2} \approx 83\%$ and $S_{CH_4} \approx 98\%$ at 400 °C (Fig. 7c), which are close to the equilibrium values, while maintaining long-term stability. These results demonstrate that tailoring the nanostructure during the deposition process and post-treatment (Section 4.2), combined with electronic interactions within the nanocomposite, is crucial for achieving high activity and stability in CO_2 methanation.

Building on the well-established role of nickel catalysts in CO_2 methanation, catalysts based on NiO_x were also produced using PECVD, giving promising results.[97] Three distinct nanocomposites were fabricated by PECVD, differing in the relative proportions of metallic Ni, NiO, Ni_2O_3 nanoparticles and a carbon matrix. Among them, the film containing the largest fraction of NiO and Ni_2O_3 nanoparticles showed the highest catalytic activity ($X_{CO_2} \approx 58\%$ and $S_{CH_4} \approx 82\%$ at 400 °C; Fig. 7c), although with some loss of performance that could be restored through recalcination in air. Interestingly, Ni^{3+} species, particularly Ni_2O_3 was found to play a crucial role in CO_2 methanation, contrary to the traditional view that metallic Ni (Ni^0) is the main active phase. The graphite-like carbon matrix present in these nanocomposites may also have a beneficial role. These findings confirm that plasma-prepared composites can behave fundamentally differently from classical Ni nanoparticles on oxide supports, highlighting the need for further research to improve the stability of these intriguing films.

Another promising group of catalysts for CO_2 utilization are FeO_x-based nanocomposites, prepared by PECVD and tested in CO_2 hydrogenation to produce CO, which is known as the reverse water–gas shift (RWGS) process.[98] Generally, all plasma-prepared thin-film FeO_x-based catalysts exhibit high selectivity toward CO (S_{CO}), although their CO_2 conversion (X_{CO_2}) varies significantly depending on the nanostructure. The most effective catalyst, containing multiple phases of Fe_2O_3 (in majority), FeO and Fe, shows superior activity (Fig. 7c) due to its ability to promote growth of carbon nanotubes (CNTs) on Fe nanoparticles during the CO_2/H_2 reaction. This, in turn, leads to the formation of nanoscale p–n heterojunctions between CNTs and Fe_2O_3 nanoparticles, producing a strong electronic effect and consequently increasing CO_2 conversion from 25% to 38% at 400 °C, approaching the equilibrium limit.

A further example of improved RWGS performance arising from electronic interactions in multicrystalline nanocomposites was also reported for thin films composed of Fe_2O_3 and CoO nanoparticles.[117] Plasma deposited (PECVD) films with varied Fe/Co ratios exhibited non-additive activity and selectivity relative to the individual oxides. Although CoO-based films alone tended to produce methane, the incorporation of Fe_2O_3 suppressed methanation and promoted CO formation, achieving up to 96% CO selectivity and 31% CO_2 conversion at 400 °C for Fe/(Fe + Co) $\approx$ 0.6–0.7 (Fig. 7c). This behavior was attributed to p–n heterojunctions that generate positive space charge in CoO and negative in Fe_2O_3 nanoparticles, thereby modifying

their catalytic properties. The mixed Fe–Co films outperformed single Fe_2O_3 films in CO production, supporting the governing role of electronic interactions in thin-film nanocomposites in shaping catalytic activity, as outlined in Section 4.3.

The above examples illustrate the potential of cold plasma deposition (PECVD) to tailor catalyst design through precise control of molecular composition and nanostructure, and as a result, improving efficiency of thermocatalytic processes. Cold plasma has proven to be an effective tool for preparing multicomponent heterostructures, such as CoO, FeO_x, and NiO_x embedded in a carbon matrix, as well as FeO_x/CoO nanohybrids. As discussed in Section 4.3, electronic interactions between different semiconductors within such hybrid catalysts can govern the catalytic activity of multicomponent systems, leading to phenomena often referred to as ''synergy'' or ''anti-synergy'' effects.[134] The latter case has been reported for nanohybrid thin films composed of CoO and WO_3 nanoparticles.[100] The heterojunctions between CoO and WO_3 induce charge accumulation within the respective nanoparticles, altering the nature of the catalytic sites. In this system, the resulting positive charge on CoO fully suppresses its methanation activity. However, this important finding provides guidance on how to optimally combine components of nanohybrids and predict their behavior based on the electronic structure of the constructing nanoparticles. It emphasizes the possibility of rational design of nanohybrid catalysts, prepared by cold plasma, through controlled electronic interactions.

In addition to thin-film nanocomposites discussed above, plasma-assisted preparation has also been successfully applied to conventional supported catalysts, demonstrating its advantage over classical thermal post-treatment that requires elevated temperatures. A notable example is the Ni/CeO_2 system prepared by incipient wetness impregnation, in which decomposition of a nickel precursor (nickel nitrate) was carried out using APPD (Section 3.4), followed by hydrogen reduction.[105] Plasma-induced decomposition introduced unique changes at the atomic-level, resulting in a smaller Ni particle size, additional Ni–O coordination and stronger metal–support interactions relative to Ni/CeO_2 subjected to conventional thermal treatment. Consequently, the plasma-prepared Ni/CeO_2 catalyst exhibited superior dispersion and significantly improved low-temperature methanation activity compared to its conventionally treated counterpart. This example further illustrates how plasma-assisted synthesis opens new pathways for tailoring active phases in catalytic nanocomposites.

5.3. Liquid-phase processes: CO_2 hydration and pollutant ozonation

The growing need for sustainable solutions to environmental challenges has led to significant research efforts exploring innovative catalytic systems in liquid-phase processes such as CO_2 capture by aqueous solvents[150,151] and wastewater ozonation treatment.[152] The conventional use of solid catalysts in particulate forms (powders, tablets, or pellets) poses operational challenges in fixed-bed absorption columns or bubble reactors, where catalysts may be used as packed beds or suspended solids.[153,154] These include uneven catalyst distribution, deactivation due to agglomeration or fouling, and difficulties in maintaining uniform contact between reactants and catalyst surfaces. Such issues become particularly important when scaling up to treat large-volume streams, where efficient gas–liquid mass transfer and catalyst separation are critical for process viability.

Plasma deposition of catalytic thin-film nanocomposites onto structured supports presents a promising approach to overcome limitations of traditional particulate catalysts.[143] Coating packing materials with thin films that serve as the gas–liquid contact interface ensures a uniform and accessible catalytic surface while overcoming issues related to handling and separation of conventional catalysts. This approach facilitates efficient catalytic reactions in gas–liquid systems while maintaining the required mass transfer characteristics. It also enables easy integration into existing reactor designs and improves operational stability.

Following these developments, recent research has demonstrated the application of nanostructured Co_3O_4-based thin-film catalysts prepared by PECVD to accelerate CO_2 hydration in water, which is the rate-limiting step in CO_2 capture by aqueous solvents.[144] This nanocatalyst, deposited on a wire mesh, enhances overall mass transfer of CO_2 by catalyzing the bicarbonate formation through a gas–solid–liquid pathway. The rate of CO_2 hydration was measured in a bubble reactor, as illustrated in Fig. 8c, under identical hydrodynamic conditions for two cases: an inert mesh and a mesh coated with the catalytic film. It was evident that the catalytic process contributes more significantly to the overall hydration rate as the CO_2 flow rate increases. This observation suggests that a higher CO_2 flow rate provides a larger contact area between CO_2 bubbles and the catalyst surface, thereby amplifying the enhancement effect. Overall, this approach resulted in up to a 40% increase in CO_2 hydration compared to the non-catalytic pathway, as shown in Fig. 7d.

Molecular studies, including XPS spectroscopy, revealed that chemisorbed water clusters on the Co_3O_4 surface serve as active sites, facilitating interaction with gaseous CO_2 and boosting hydration kinetics leading to bicarbonate formation (Fig. 7e). Although the experiments were performed at a small laboratory scale in a bubble reactor using a single piece of catalytic mesh, this approach offers promising prospects for transferring to large-scale absorption columns with structured packing. As previously mentioned, the cold-plasma deposition technique is scalable and enables uniform Co_3O_4 thin-film coatings on structured packings, providing a feasible way for integrating catalysts into the design of industrial absorption columns.

Building on the approach used to enhance CO_2 hydration, catalytic ozonation – which is widely used to degrade organic pollutants in wastewater – also shows promising potential for plasma-deposited thin-film nanocomposites. In this context, tungsten-based thin-film catalysts deposited by PECVD on fine meshes enable efficient contact between ozone gas and the catalyst, while being integrated within the special design of the bubble column (Fig. 8d).[145] These W-based thin films containing

varied amounts of WC, WO_2 and WO_3 in a carbon matrix exhibited different activities and stabilities in the catalytic ozonation of the textile dye Reactive Black 5 (RB5) in simulated wastewater. Their performance was assessed by determining the overall rate constant for RB5 decolorization. The most active nanocomposite was shown to achieve an enhancement factor of 1.47 compared with single ozonation, confirming the improved efficiency of dye degradation in the presence of this catalyst. However, the nanostructure has not yet been investigated and the specific roles of WC, WO_2 and WO_3 have not been explicitly confirmed. Moreover, the most active catalyst was applied to decolorize real textile wastewater containing RB5 and also exhibited a much higher decolorization rate than single ozonation. A comparison of dye degradation rates for these two cases (simulated *vs.* real wastewater) is presented in Fig. 7f.

Similarly, plasma-deposited Co_3O_4 and Fe_2O_3 thin-film catalysts demonstrated activity in catalytic ozonation, enhancing the removal of dyes and degradation of by-products compared to single ozonation across a broad pH range.[146] As shown in Fig. 7g, these nanocomposites exhibited kinetic rates surpassing classical ozonation, particularly under alkaline conditions, with Co_3O_4 and Fe_2O_3 films showing 1.48-fold and 1.66-fold enhancements, respectively, relative to single ozonation. The use of these catalysts also allowed for decreasing the required ozone dosage, confirming improved process efficiency.

The results presented above illustrate that plasma-deposited thin-film nanocomposites combine catalytic enhancement with favorable hydrodynamics in a manner that is not accessible to conventional packed beds or suspended powders. The catalyst becomes an integral part of the gas–liquid contacting elements, which is particularly advantageous for scaling up processes such as CO_2 absorption or catalytic ozonation.

From a technical point of view, the use of catalysts deposited as thin films on wire mesh enabled the development of an innovative design of catalytic bubble column.[145,146] The proposed, patented construction incorporates baffles filled with mesh coated with a thin-film catalyst.[155] As a result, the gas ascending the column must pass through these meshes, ensuring its direct contact with the catalytic surface. This arrangement will enhance ozone decomposition and pollutant degradation. Additionally, the design of this reactor provides better hydrodynamics compared to configurations without baffles, improving gas–liquid contact and mass transfer rates, which together increase the overall efficiency compared to single ozonation (*i.e.* without any baffles and meshes). These findings highlight the practical potential of plasma-deposited nanocomposites for advanced wastewater treatment applications. However, it should be noted that the reported improvement in wastewater ozonation in comparison to single ozonation does not arise solely from catalysis,[145,146] as in the case of CO_2 hydration,[144] but represents a combined effect of improved hydrodynamics and catalytic activity. Notably, a catalytic effect is evident despite this combined contribution, as bare kanthal steel meshes calcined to form an Al_2O_3 layer consistently performed worse than identical meshes coated with plasma-deposited Co_3O_4 or Fe_2O_3 films (Fig. 7g).

5.4. Cold plasma-deposited *vs.* conventional catalysts

The broad prospects for thin-film nanocomposites with catalytic properties produced using cold plasma deposition methods – highlighted several times throughout this review – have become more tangible when the innovative features and catalytic performance of these materials are compared with those of similar catalysts produced by conventional methods. Such a comparison is inherently limited by the fact that plasma-deposited catalysts are not yet practically implemented in industry. Consequently, assessments of large-scale production costs or catalytic performance under different packing configurations and process conditions must rely on hypothetical estimates and laboratory-scale data. Nevertheless, comparative analysis of plasma-deposited catalysts against conventional catalysts used in similar thermocatalytic processes enables a more comprehensive and objective evaluation of their potential.

Table 2 summarizes the key characteristics of both catalyst groups. The comparison is primarily qualitative and is based on literature reports describing conventional catalyst synthesis methods, such as impregnation, sol–gel, hydrothermal and solvothermal techniques, and deposition precipitation methods,[156,157] as well as approaches specifically designed to produce coatings on structured supports or microreactor surfaces.[158–160] In addition, published discussions on the advantages and limitations of thin films deposited by cold plasma are considered.[38,161]

The data presented in Table 2 clearly demonstrate the high utility of plasma deposition technology, particularly for producing thin-film catalysts on the surfaces of structured supports. The ability to deposit very thin films on three-dimensional surfaces distinctly differentiates this technology from conventional catalyst-coating methods and provides chemical engineers with a valuable tool for the design of structured reactors. Moreover, beyond the broad possibilities for tailoring film properties – offering significant flexibility in achieving desired catalytic activity – the markedly lower consumption of raw materials and substantially reduced energy requirements relative to conventional catalyst synthesis routes are noteworthy advantages. Conventional methods often involve multistep procedures and typically require energy-intensive treatments for solvent evaporation and high-temperature calcination. These fundamental differences in material and energy demands are reflected in estimated catalyst production costs.

Accurately determining total production costs depends on numerous factors, including catalyst composition, performance, production scale, equipment depreciation, life-cycle assessment (LCA), *etc.*, making such evaluations complex and frequently ambiguous.[162] An additional challenge in comparing conventional catalysts with those produced by cold plasma deposition is the selection of an appropriate baseline metric. Catalyst mass, commonly used for conventional materials, is not suitable in this case. Instead, geometric surface area can be proposed as a more appropriate comparative parameter, enabling a more objective assessment of manufacturing costs for both catalyst types. By knowing the density of a conventional catalyst and the average size of its constituent particles

Table 2 Comparison of key criteria characterizing conventional and cold plasma-deposited catalysts

Criterion	Classical (impregnation, sol–gel, hydrothermal, solvothermal, and precipitation)	Cold plasma thin-film deposition
Tailoring of molecular, nanostructural and electronic properties	Clearly limited	Very wide possibilities
Form of catalyst	Powder/particles, thick coatings; coated onto supports	Direct thin film on supports
Active phase dispersion/distribution	Depends on precursors and supports	Tailorable *via* plasma parameters
Film thickness control	Indirect; depends on subsequent deposition; generally low precision	Direct; nanometer precision
3D conformality	Limited; may block fine features	Excellent; driven by plasma species
Materials consumption	Generally high	Very low
Thermal load	Often requires high temperature calcination	Can operate at lower temperatures
Energy consumption	Medium or high	Low
Scalability	Well-established	Growing; possibility of adopting industrial cold plasma systems
Cost (catalysts based on non-noble metals)	Average 47 $ per m^2 of geometric surface area	Average 5.3 $ per m^2 of geometric surface area

(*e.g.*, spherical pellets), the ratio of geometric surface area to mass can be calculated and compared with the cost of producing an equivalent surface area coated with a similar type of catalyst *via* plasma deposition. Table 2 presents approximate cost estimates for catalysts based on non-noble metal oxides produced using a conventional method[163] and cold plasma deposition.[39,164] Overall, the substantially lower estimated cost of plasma-deposited nanocatalysts, combined with their additional advantages discussed above, reinforces their innovative character and considerable application potential.

Catalytic activity is another critical factor in evaluating catalyst usefulness. CO_2 hydrogenation was selected as a model process for comparison, as it is one of the most actively studied processes in the field of catalyst applications and has also been relatively well investigated for plasma-deposited thin-film nanocatalysts (Section 5.2). For this process, CO_2 conversion (X_{CO_2}) and selectivity toward methane (S_{CH_4}) or carbon monoxide (S_{CO}) were compared for selected conventional and plasma-deposited catalysts in two categories: cobalt-based catalysts, where methanation reaction predominates and CH_4 is the main product, and iron-based catalysts, where the reverse water-gas shift reaction dominates, yielding CO (Table 3). Although the catalytic tests were conducted under different reaction conditions, such as temperature, pressure, molar ratio of reagents and weight hourly space velocity (WHSV) – complicating direct quantitative comparisons – the plasma-deposited catalysts generally exhibit very high efficiency, often surpassing that of their conventional counterparts. This performance strongly underscores their promising industrial potential.

6. Summary and perspectives

It is safe to say that the technology of thin-film deposition using cold plasma, known for a very long time, is currently experiencing a new renaissance. This is primarily due to the recognition of the enormous potential of this technology and the recent attempts to utilize it for the rational production of entirely new nanocomposite materials exhibiting catalytic activity. The search for new nanocatalysts with high efficiency, selectivity, and durability, dedicated to specific catalytic processes, while simultaneously obtaining these materials in the form required by modern structured reactor designs, is the driving force behind the activities and progress recently observed in adapting cold plasma deposition methods to address these challenges.

This review introduces the concept underlying the use of cold plasma technology to fabricate thin-film nanocomposites for heterogeneous thermocatalysis, presents the current state of knowledge in this field, and outlines the future prospects of this approach. After a brief review of the historical foundations of this technology, the most important innovations in cold plasma deposition methods are discussed. Particular attention is given to the ''classical'' low-pressure plasma enhanced chemical vapor deposition (PECVD) method, which still holds a leading position among these techniques. In recent years, it has developed intensively thanks to the introduction of innovative methods for delivering precursors to the plasma region, significantly expanding its capabilities. The following part focuses on atmospheric-pressure cold plasma (APPD), which is now increasingly being used in film deposition beyond traditional surface treatment. The latest achievements of the plasma-enhanced atomic layer deposition (PEALD) method have also been addressed. After a major step forward enabled by an ingenious modification – spatial PEALD – this method is no longer merely a sophisticated research curiosity, but is beginning to demonstrate real application potential.

The development of plasma deposition methods for thin films and the advances in reactor design are only one aspect of the current boom in cold plasma technology. Another crucial aspect, discussed in the next part of this review, is the significant progress in tailoring the molecular structure, nanostructure, and electronic structure of deposited films through rational control of their production process.

By selecting an appropriate precursor structure and controlling the deposition parameters and possible post-treatments, we are increasingly close to realizing a designed nanocomposite structure with the expected catalytic properties.

Table 3 Comparison of CO_2 conversion and selectivity toward CH_4 or CO in methanation or reverse water-gas shift (RWGS) reactions, respectively, for selected conventional and plasma-deposited catalysts with cobalt-based (for methanation) or iron-based (for RWGS) structures

Catalyst	Preparation method	Operational conditions	CO_2 conversion X_{CO_2} [%]	Selectivity S_{CH_4} or S_{CO} [%]	Ref.
CO_2 methanation: $CO_2 + 4H_2 \Leftrightarrow CH_4 + 2H_2O$; selectivity for S_{CH_4}					
Co/ZrO_2	Acid-assisted incipient wetness impregnation	400 °C 3 MPa, $H_2:CO_2 = 4:1$ WHSV = 7200 mL g_{cat}^{-1} h^{-1}	85	99	165
$Co/Ce_{0.8}Zr_{0.2}O_2$	Conventional co-precipitation	320 °C 1.5 MPa, $H_2:CO_2 = 3:1$ WHSV = 15 000 mL g_{cat}^{-1} h^{-1}	81.2	99	166
Co/Al_2O_3	Incipient impregnation	400 °C 0.1 WHSV = 16 000 mL g_{cat}^{-1} h^{-1}	~82	~98	167
Bare CoO NPs	Hydrothermal method	300 °C 0.1 MPa, $H_2:CO_2 = 3:1$ WHSV – not provided	55	97	168
Co/Al_2O_3	Wet impregnation	400 °C 0.1 MPa, $H_2:CO_2 = 5:1$ (diluted in N_2) WHSV = 55 000 mL g_{cat}^{-1} h^{-1}	~56	~88	169
CoO-based thin films	PECVD	400 °C 0.1 MPa, $H_2:CO_2 = 4:1$ WHSV = 150 000 mL g_{cat}^{-1} h^{-1}	83	98	117
Reverse water-gas shift reaction: $CO_2 + H_2 \Leftrightarrow CO + H_2O$; selectivity for S_{CO}					
Fe-oxide	Co-precipitation	600 °C 0.1 MPa, $H_2:CO_2 = 1:1$ WHSV = 24 000 mL g_{cat}^{-1} h^{-1}	31	>85	170
Fe_3O_4	Physical processing of commercial powder (Fe_3O_4, Fe_3C)	480 °C 0.1 MPa, $H_2:CO_2 = 4:1$ (diluted in He) WHSV = 45 000 mL g_{cat}^{-1} h^{-1}	34	98.6	171
Fe/Al_2O_3	Sequential wet impregnation	400 °C	30	74	172
$2.5\%CsFe/Al_2O_3$		0.1 MPa, $H_2:CO_2 = 4:1$ WHSV = 12 000 mL g_{cat}^{-1} h^{-1}	37	79	
$10Fe/SiO_2$	Incipient wetness impregnation	300 °C	~(3–4)	~46	173
$2Na10Fe/SiO_2$		3 MPa, $H_2:CO_2 = 3:1$ WHSV = 1600 mL g_{cat}^{-1} h^{-1}	~2	~94	
FeO_x/CNT thin films	PECVD	400 °C 0.1 MPa, $H_2:CO_2 = 4:1$ WHSV = 150 000 mL g_{cat}^{-1} h^{-1}	39	94	98

This review also presents a systematic overview of catalytic studies conducted in recent years involving plasma-deposited nanocomposites. On the one hand, these materials were already the result of at least partial design and implementation of the intended structure; on the other hand, they were produced as thin films that meet the requirements of 3D structured packings. As a representative example, films deposited from a cobalt metal–organic precursor can be mentioned. Their structure can be readily manipulated to obtain a nanocomposite containing CoO nanoparticles in a carbon matrix or, alternatively, Co_3O_4 nanoparticles. These two types of films exhibited high catalytic activity, albeit in completely different processes: CoO-based films proved excellent in CO_2 methanation, while Co_3O_4-based films demonstrated excellent activity in the combustion of volatile hydrocarbons.

When discussing the possibility of tailoring the structure of films – particularly their electronic structure, which is crucial for catalytic properties – attention was also given to another important aspect, revealed recently: the ability to use cold plasma deposition to produce nanocomposite films with nanoscale heterojunctions that control thermocatalytic activity. The concept of such nanocatalytic systems holds enormous application potential.

Despite the significant progress achieved in recent years in cold plasma deposition technology, and the increasingly successful attempts to design the structure of prepared films, we are still far from the ultimate goal: developing a complete procedure for achieving the desired catalytic activity for a given process by tailoring the electronic structure of a nanocomposite (resulting from an appropriately designed molecular structure and nanostructure) and implementing such a system precisely through the selection of the plasma method and deposition conditions. In pursuing this goal, the following should be considered the main research challenges in the near future:

(1) Further systematic exploration of the correlation between catalytic activity, film structure, and fabrication conditions: particular attention should be paid to nanoscale heterojunctions, which have recently generated considerable interest and open prospects for fully targeted control of catalytic properties;

(2) Development of advanced methods for introducing precursors into the plasma reactor, for example, in the form of an aerosol or an atomized jet generated by thermal plasma: this

would significantly broaden the possibilities for achieving the designed molecular structure of the film at the precursor-selection level and at the same time allow the elimination of metal–organic precursors, which are often cumbersome to use, especially in co-deposition, not to mention their generally high cost. Abandoning metal–organic precursors would also facilitate moving beyond carbon matrices and enable the production of alternative matrices, *e.g.*, silicon-based ones, thus significantly expanding the range of potential nanocomposite catalytic materials;

(3) With regard to nanocomposite film matrices, it is essential to intensify research on their nanomembrane structure, beyond issues related to their electronic interactions with embedded nanoparticles. There is already compelling evidence indicating that a thin nanocomposite film – *e.g.*, a carbon matrix containing CoO nanoparticles – acts catalytically not only on its surface but throughout its entire volume. The thicker the film, the greater the conversion. Reactants diffusing into the bulk of the film utilize CoO nanoparticles located within it, not only those exposed at the outer surface. This new insight reinforces the belief in the unique properties of thin films deposited in cold plasma;

(4) Intensifying efforts to scale up from laboratory to industrial production: moving substrates, roll-to-roll systems, and 3D printing combined with plasma deposition of nanocatalyst films are examples of solutions requiring further intensive development before thin-film cold plasma technology can fully enter large-scale production of structured packings for the chemical industry.

In summary, we can once again emphasize the broad prospects offered by cold plasma technology for producing entirely new thin-film nanohybrid catalytic materials and encourage further research in this field, both in basic sciences and in application-oriented studies on advanced catalytic processes.

Conflicts of interest

There are no conflicts to declare.

Data availability

No primary research results have been included and no new data were generated or analyzed as part of this review.

Notes and references

1 S. Wacławek, V. V. T. Padil and M. Černik, *Ecol. Chem. Eng.*, 2018, **25**, 9–34.
2 B. R. Cuenya, *Thin Solid Films*, 2010, **518**, 3127–3150.
3 P. S. F. Mendes, J. M. Silva, M. F. Ribeiro, A. Daudin and C. Bouchy, *Catal. Today*, 2020, **356**, 260–270.
4 ed. U. Heiz and U. Landman, *Nanocatalysis*, Springer, Berlin, 2006.
5 S. Olveira, S. P. Förster and S. Seeger, *J. Nanotechnol.*, 2014, **2014**, 324089.
6 T. Ishida, T. Mutayama, A. Taketoshi and M. Haruta, *Chem. Rev.*, 2020, **120**, 465–525.
7 D. Astruc, *Chem. Rev.*, 2020, **120**, 461–463.
8 F. de Clippel, M. Dusselier, S. Van de Vyver, L. Peng, P. A. Jacobs and B. F. Sels, *Green Chem.*, 2013, **15**, 1398–1430.
9 K. Sahoo, T. R. Gazi, S. Roy and I. Chakraborty, *Commun. Chem.*, 2023, **6**, 157.
10 T. W. van Deelen, C. H. Mejia and K. P. de Jong, *Nat. Catal.*, 2019, **2**, 955–970.
11 Y. Li, Y. Zhang, K. Qian and W. Huang, *ACS Catal.*, 2022, **12**, 1268–1287.
12 X. Yu, J. Deng, Y. Liu, L. Jing, Z. Hou, W. Pei and H. Dai, *Catalysts*, 2022, **12**, 1239.
13 A. O. Ibrahim, A. Halilu, W. M. A. W. Daud, M. F. A. Patah and J. C. Juan, *Mol. Catal.*, 2022, **529**, 112535.
14 B. Li, L. Li, G. Zhang, L. Sun, J. Wu, L. Liu, J. Liu, S. Liu, W. Xue, Q. Ye, N. Zhu, Z. Dang, T. Wang and P. Wu, *ACS Catal.*, 2025, **15**, 10239–10270.
15 J. Shi, *Chem. Rev.*, 2013, **113**, 2139–2181.
16 N. D. Cuong and D. T. Quang, *Vietnam J. Chem.*, 2020, **58**, 434–463.
17 J. H. Carter, S. Althahban, E. Nowicka, S. J. Freakley, D. J. Morgan, P. M. Shah, S. Golunski, C. J. Kiely and G. J. Hutchings, *ACS Catal.*, 2016, **6**, 6623–6633.
18 L. Pastor-Perez, S. Gu, A. Sepulveda-Escribano and T. R. Reina, *Int. J. Hydrogen Energy*, 2019, **44**, 4011–4019.
19 N. Baig, I. Kammakakam and W. Falath, *Mater. Adv.*, 2021, **2**, 1821–1871.
20 T. A. Rasheed, B. Afotey and D. A. Anang, *Int. J. Thin Film Sci. Technol.*, 2023, **13**, 27–36.
21 J. Tyczkowski, in *Plasma Science and Technology - Progress in Physical States and Chemical Reactions*, ed. T. Mieno, InTech, London, 2016, ch. 3, pp. 53–93.
22 Z. Wang, Y. Zhang, E. C. Neyts, X. Cao, X. Zhang, B. W. L. Jang and C. J. Liu, *ACS Catal.*, 2018, **8**, 2093–2110.
23 L. Di, J. Zhang, X. Zhang, H. Wang, H. Li, Y. Li and D. Bu, *J. Phys. D: Appl. Phys.*, 2021, **54**, 333001.
24 J. Tyczkowski and H. Kierzkowska-Pawlak, *Catalysts*, 2022, **12**, 75.
25 F. Shi, J. Jiang, X. Wang, Y. Gao, C. Chen, G. Chen, N. Dudko, A. A. Nevar and D. Zhang, *Chem. Commun.*, 2024, **60**, 2700–2715.
26 J. Tyczkowski, H. Kierzkowska-Pawlak, R. Kapica, J. Balcerzak and J. Sielski, *Catal. Today*, 2019, **337**, 44–54.
27 M. P. V. Wilde, *Ber. Dtsch. Chem. Ges.*, 1874, **7**, 352–357.
28 P. Thenard and A. Thenard, *C. R. Hebd. Seances Acad. Sci.*, 1874, **78**, 219.
29 J. Goodman, *J. Polym. Sci.*, 1960, **44**, 551–552.
30 ed. H. Biederman, *Plasma Polymer Films*, Imperial College Press, London, 2004.
31 H. K. Yasuda, *Plasma Polymerization*, Academic Press, Orlando, 1985.
32 A. Bradley and J. P. Hammes, *J. Electrochem. Soc.*, 1963, **110**, 15–22.
33 H. F. Sterling and R. C. G. Swann, *Solid-State Electron.*, 1965, **8**, 653–654.
34 M. S. A. Kamel, M. Oelgemöller and M. V. Jacob, *Renew. Sustain. Energy Rev.*, 2024, **203**, 114740.
35 M. Saeed, Y. Alshammari, S. A. Majeed and E. Al-Nasrallah, *Molecules*, 2020, **25**, 3856.
36 H. Pedersen, S. T. Barry and J. Sundqvist, *J. Vac. Sci. Technol., A*, 2021, **39**, 051001.
37 A. Loesch-Zhang, A. Geissler and M. Biesalski, *Plasma Process Polym.*, 2023, **20**, e2300016.
38 R. Snyders, D. Hegemann, D. Thiry, O. Zabeida, J. Klemberg-Sapieha and L. Martinu, *Plasma Sources Sci. Technol.*, 2023, **32**, 074001.
39 L. Martinu, O. Zabeida and J. E. Klemberg-Sapieha, in *Handbook of Deposition Technologies for Films and Coatings*, ed. P. M. Martin, William Andrew Publ., Norwich, 3rd edn, 2010, ch. 9, pp. 392–465.
40 J. Tyczkowski, in *Electrochemical Cells – New Advances in Fundamental Researches and Applications*, ed. Y. Shao, InTech, London, 2012, ch. 5, pp. 105–138.
41 A. M. Wróbel and M. R. Wertheimer, in *Plasma Deposition, Treatment, and Etching of Polymers*, ed. R. d'Agostino, Academic Press, San Diego, 1990, ch. 3, pp. 163–268.
42 N. Morosoff, D. L. Patel, P. S. Lugg and A. L. Crumbliss, *J. Appl. Polym. Sci: Appl. Polym. Symp.*, 1984, **38**, 83–97.
43 Y. Osada, A. Mizumoto and H. Tsuruta, *J. Macromol. Sci.–Chem.*, 1987, **A24**, 403–418.
44 H. Holzschuh, C. Oehr, H. Shur and A. Weber, *Mod. Phys. Lett. B*, 1988, **2**, 1253–1257.
45 H. Suhr, A. Etspüler, E. Feurer and C. Oehr, *Plasma Chem. Plasma Process.*, 1988, **8**, 9–17.

46 A. Weber and H. Suhr, *Mod. Phys. Lett. B*, 1989, **3**, 1001–1008.
47 Y. Matatov-Meytal and M. Sheintuch, *Appl. Catal., A*, 2002, **231**, 1–16.
48 M. V. Twigg and J. T. Richardson, *Chem. Eng. Res. Des.*, 2002, **80**, 183–189.
49 J. Tyczkowski, R. Kapica and J. Łojewska, *Thin Solid Films*, 2007, **515**, 6590–6595.
50 J. Tyczkowski and R. Kapica, *Pol. J. Chem. Technol.*, 2007, **9**, 36–42.
51 J. Łojewska, A. Kołodziej, T. Łojewski, R. Kapica and J. Tyczkowski, *Appl. Catal., A*, 2009, **366**, 206–211.
52 A. Kołodziej, J. Łojewska, J. Tyczkowski, P. Jodłowski, W. Redzynia, M. Iwaniszyn, S. Zapotoczny and P. Kuśtrowski, *Chem. Eng. J.*, 2012, **200–202**, 329–337.
53 T. Dufour, *Polymers*, 2023, **15**, 3607.
54 P. Mandracci and P. Rivolo, *Coatings*, 2023, **13**, 1075.
55 Z. Wu, Y. Zhang, L. Li, Y. Zhao, Y. Shen, S. Wang and G. Shao, *J. Mater. Chem. A*, 2020, **8**, 23248–23256.
56 Y. Zhao, X. Zhou, S. Gao, S. Song and Y. Zhao, *Plasma Sci. Technol.*, 2024, **26**, 075402.
57 Y. Liu, F. M. Elam, E. Zoethout, S. A. Starostin, M. C. M. van de Sanden and H. W. de Vries, *J. Phys. D: Appl. Phys.*, 2019, **52**, 355201.
58 R. Pribyl, S. Kelarova, M. Karkus and V. Bursikova, *Carbon Trends*, 2024, **17**, 100416.
59 B. Panek and H. Kierzkowska-Pawlak, *Plasma Phys. Control. Fusion*, 2025, **67**, 055034.
60 Y. Kim, M. Lee and Y. J. Kim, *Micromachines*, 2019, **10**, 689.
61 R. S. Matos, N. S. Ferreira, S. Tălu, A. Ghaderi, S. Solyamani, M. A. Pires, E. A. Sanches and H. D. da Fonseca Filho, *Symmetry*, 2022, **14**, 2675.
62 S. Rezaee, M. Mardani, A. Shafiekhani, A. Arman and C. Luna, *Surf. Interfaces*, 2024, **52**, 104820.
63 L. P. G. Oliveira, R. P. Ribeiro, J. R. R. Bortolete, N. C. Cruz and E. C. Rangel, *Mater. Res.*, 2021, **24**(suppl. 1), e20210058.
64 P. Souček, J. Daniel, J. Hnilica, K. Bernátová, L. Zábranský, V. Buršiková, M. Stupavská and P. Vašina, *Surf. Coat. Technol.*, 2017, **311**, 257–267.
65 C. Nouvellon, R. Belchi, L. Libralesso, O. Douhéret, R. Lazzaroni, R. Snyders and D. Thiry, *Thin Solid Films*, 2017, **630**, 79–85.
66 G. Carnide, C. Simonnet, D. Parmar, Z. Zavvou, H. Klein, R. Conan, V. Pozsgay, T. Verdier, C. Villeneuve-Faure, M. L. Kahn, L. Stafford and R. Clergereaux, *Plasma Chem. Plasma Process.*, 2024, **44**, 1343–1356.
67 C. Guyon, A. Barkallah, F. Rousseau, K. Giffard, D. Morvan and M. Tatoulian, *Surf. Coat. Technol.*, 2011, **206**, 1673–1679.
68 G. L. Chen, C. Guyon, Z. X. Zhang, B. Da Silva, P. Da Costa, S. Ognier, D. Bonn and M. Tatoulian, *Microfluid. Nanofluid.*, 2014, **16**, 141–148.
69 M. Mitronika, J. Profili, A. Goullet, N. Gautier, N. Stephant, L. Stafford, A. Granier and M. Richard-Plouet, *J. Phys. D: Appl. Phys.*, 2021, **54**, 085206.
70 G. Mauer, M. Gindrat and M. F. Smith, *J. Therm. Spray Technol.*, 2016, **25**, 1383–1388.
71 D. Ivchenko, PhD thesis, Université de Limoges, 2018.
72 M. Gindrat, H. M. Höhle, K. von Niessen, P. Guittienne, D. Grange and C. Hollenstein, *J. Therm. Spray Technol.*, 2011, **20**, 882–887.
73 C. Carra, E. Dell'Orto, V. Morandi and C. Riccardi, *Coatings*, 2020, **10**, 788.
74 C. Piferi, C. Carra, K. Bazaka, H. E. Roman, E. C. Dell'Orto, V. Morandi, I. Levchenko and C. Riccardi, *Nanomaterials*, 2022, **12**, 533.
75 A. Uricchio and F. Fanelli, *Processes*, 2021, **9**, 2069.
76 F. Palumbo, C. Lo Porto, F. Fracassi and P. Favia, *Coatings*, 2020, **10**, 440.
77 R. Mangan, R. Clergereau, C. Villeneuve-Faure, B. Lantin, G. Carnide, P. Raynaud and N. Naude, *Eur. Phys. J.: Appl. Phys.*, 2022, **97**, 37.
78 J. Mallmann, J. B. Chemin, D. C. Morcoso, A. M. Philippe, S. Bulou, N. Chaabane, F. Rouillard, P. Choquet and N. D. Boscher, *ACS Appl. Energy Mater.*, 2025, **8**, 7038–7051.
79 J. L. Hodgkinson, H. M. Yates, A. Walter, D. Sacchetto, S. J. Moonb and S. Nicolay, *J. Mater. Chem. C*, 2018, **6**, 1988–1995.
80 V. H. Nguyen, A. Sekkat, C. A. M. de la Huerta, F. Zoubian, C. Crivello, J. Rubio-Zuazo, M. Jaffal, M. Bonvalot, C. Vallée, O. Aubry, H. Rabat, D. Hong and D. Muñoz-Rojas, *Chem. Mater.*, 2020, **32**, 5153–5161.
81 R. W. Johnson, A. Hultqvist and S. F. Bent, *Mater. Today*, 2014, **17**, 236–246.
82 H. C. M. Knoops, T. Faraz, K. Arts and W. M. M. Kessels, *J. Vac. Sci. Technol., A*, 2019, **37**, 030902.
83 P. O. Oviroh, R. Akbarzadeh, D. Pan, R. A. M. Coetzee and T. C. Jen, *Sci. Technol. Adv. Mater.*, 2019, **20**, 465–496.
84 J. Shen, F. Roozenboom and A. Mameli, *ALDJ*, 2023, **1**, 1–11.
85 B. J. O'Neill, D. H. K. Jackson, J. Lee, C. Canlas, P. C. Stair, C. L. Marshall, J. W. Elam, T. F. Kuech, J. A. Dumesic and G. W. Huber, *ACS Catal.*, 2015, **5**, 1804–1825.
86 A. Illiberi, I. Katsouras, S. Gazibegovic, B. Cobb, E. Nekovic, W. van Boekel, C. Frijters, J. Maas, F. Roozeboom, Y. Cteyghton, P. Poodt and G. Gelinck, *J. Vac. Sci. Technol. A*, 2018, **36**, 04F401.
87 M. van de Poll, J. Shen, J. Hilfiker, M. Verheijen, P. Poodt, F. van den Bruele, W. Kessels and B. Macco, *J. Phys. Chem. C*, 2025, **129**, 2210–3320.
88 M. Chen, M. P. Nijboer, A. Y. Kovalgin, A. Nijmeijer, F. Roozeboom and M. W. J. Luiten-Olieman, *Dalton Trans.*, 2023, **52**, 10254–10277.
89 K. Cao, J. Cai, X. Liu and R. Chen, *J. Vac. Sci. Technol., A*, 2018, **36**, 0010801.
90 T. Faraz, M. van Druden, H. C. M. Knoops, A. Mallikarjunan, I. Buchanan, D. M. Hausmann, J. Henri and W. M. M. Kessels, *ACS Appl. Mater. Interfaces*, 2017, **9**, 1858–1869.
91 L. Xin, H. Yongqiang and J. Husheng, *Rare Met. Mater. Eng.*, 2017, **46**, 339–343.
92 C. R. Tubio, J. Azuaje, L. Escalante, A. Coelho, F. Guitián, E. Sotelo and A. Gil, *J. Catal.*, 2016, **334**, 110–115.
93 C. Parra-Cabrera, C. Achille, S. Kuhn and R. Ameloot, *Chem. Soc. Rev.*, 2018, **47**, 209–230.
94 J. Lojewska, A. Kolodziej, R. Kapica, A. Knapik and J. Tyczkowski, *Catal. Today*, 2009, **147S**, 594–598.
95 R. Kapica, W. Redzynia, M. Kozanecki, M. M. Chemini, J. Sielski, S. M. Kuberski and J. Tyczkowski, *Mater. Sci.*, 2013, **19**, 270–276.
96 L. Wang, T. P. Tran, D. V. Vo, M. Sakurai and H. Kameyama, *Appl. Catal., A*, 2008, **350**, 150–156.
97 M. Smolarek, H. Kierzkowska-Pawlak, R. Kapica, M. Fronczak, M. Sitarz, M. Leśniak and J. Tyczkowski, *Catalysts*, 2021, **11**, 905.
98 B. Panek, H. Kierzkowska-Pawlak, P. Uznański, S. Nagy, V. Nagy-Trembošová and J. Tyczkowski, *Catalysts*, 2023, **13**, 1302.
99 H. Kierzkowska-Pawlak, M. Ryba, M. Fronczak, R. Kapica, J. Sielski, M. Sitarz, P. Zając, K. Łyszczarz and J. Tyczkowski, *Catalysts*, 2021, **11**, 883.
100 B. Panek, H. Kierzkowska-Pawlak, P. Uznański and J. Tyczkowski, *Small*, 2025, e13289.
101 A. Liguori, H. Xu, D. Hazarika and M. Hakkarainen, *ACS Appl. Polym. Mater.*, 2023, **5**, 8506–8517.
102 C. Lo Porto, M. Dell'Edera, I. De Pasquale, A. Milella, F. Fracassi, M. L. Curri, R. Comparelli and F. Palumbo, *Nanomaterials*, 2022, **12**, 3758.
103 S. Weeks, G. Nowling, N. Fuchigami, M. Bowes and K. Littau, *J. Vac. Sci. Technol. A*, 2016, **34**, 01A140.
104 H. Kazari, E. Pajootan, M. Sowa, S. Coulombe and P. Hubert, *J. Energy Storage*, 2023, **64**, 107049.
105 N. Rui, X. Zhang, F. Zhang, Z. Liu, X. Cao, Z. Xie, R. Zou, S. D. Senanayake, Y. Yang, J. A. Rodriguez and C. J. Liu, *Appl. Catal., B*, 2021, **282**, 119581.
106 D. Vollath, *KONA*, 2007, **25**, 39–55.
107 E. Thimsen, U. R. Kortshagen and E. S. Aydil, *J. Phys. D: Appl. Phys.*, 2015, **48**, 314004.
108 N. Joshi and S. Loganathan, *Catalysts*, 2024, **14**, 802.
109 D. Wang, T. Zhou, S. Tang, D. Tian, H. Zhang, Q. Chen and Z. Liua, *J. Vac. Sci. Technol., A*, 2022, **40**, 062404.
110 R. Fang, C. Yao, Q. Wang, F. Feng, C. Lu, Q. Zhang and X. Li, *Catal. Rev.*, 2025, 1–62.
111 S. Yao, Y. Ma, T. Xu, Z. Wang, P. Lv, J. Zheng, C. Ma, K. Yu, W. Wei and K. (Ken) Ostrikov, *Carbon*, 2021, **171**, 524–531.
112 X. Lan, G. Li, R. Jin, X. Li and J. Zheng, *Chem. Eng. J.*, 2022, **450**, 138225.
113 S. Banerjee, E. Adhikari, P. Sapkota, A. Sebastian and S. Ptasinska, *Materials*, 2020, **13**, 2931.
114 A. Kafizas, C. J. Carmalt and I. P. Parkin, *Coord. Chem. Rev.*, 2013, **257**, 2073–2119.

115 C. A. Beaudette, J. T. Held, K. A. Mkhoyan and U. R. Kortshagen, *ACS Omega*, 2020, **5**, 21853–21861.
116 S. Yeo, D. K. Nandi, R. Rahul, T. H. Kim, B. Shong, Y. Jang, J. S. Bae, J. W. Han, S. H. Kim and H. Kim, *Appl. Surf. Sci.*, 2018, **459**, 596–605.
117 N. Mohammadpour, H. Kierzkowska-Pawlak, J. Balcerzak, P. Uznański and J. Tyczkowski, *Catalysts*, 2024, **14**, 38.
118 J. Tyczkowski, R. Kapica, M. Kozanecki, H. Kierzkowska-Pawlak, J. Sielski, T. Aoki and H. Mimura, *Mater. Design.*, 2022, **222**, 111095.
119 B. Singh, T. Fischer and S. Mathur, *J. Mater. Chem. A*, 2025, **13**, 20104–20142.
120 S. Greenhorn, E. Bano, V. Stambouli and K. Zekentes, *Materials*, 2024, **17**, 1135.
121 E. Ermakova, K. Mogilnikov, I. Asanov, A. Fedorenko, I. Yushina, V. Kichay, E. Maksimovskiy and M. Kosinova, *Coatings*, 2022, **12**, 1767.
122 H. Kierzkowska-Pawlak, J. Tyczkowski, J. Balcerzak and P. Tracz, *Catal. Today*, 2019, **337**, 162–170.
123 S. Saha and D. Das, *Appl. Surf. Sci.*, 2022, **596**, 153638.
124 H. Sheng, W. Xiong, S. Zheng, C. Chen, S. He and Q. Cheng, *Carbon Lett.*, 2021, **31**, 929–939.
125 J. Che, P. Yi, L. Peng and X. Lai, *Int. J. Hydrogen Energy*, 2020, **45**, 16277–16286.
126 Y. Zhai, W. Wang, R. Chen, T. Yu, X. Zheng, H. Shao, D. Shang, L. Li and L. Filipovic, *Adv. Intell. Discov.*, 2025, **0**, e2500074.
127 I. Hinkov, K. Pashova and S. Farhat, *DRM*, 2019, **93**, 84–95.
128 T. Gergs, T. Mussenbrock and J. Trieschmann, *J. Phys. D: Appl. Phys.*, 2023, **56**, 194001.
129 ed. K. Philippot and A. Roucoux, *Nanoparticles in Catalysis*, Wiley-VCH, Weinheim, 2021.
130 A. Ghaderi, A. Shafiekhani, S. Solaymani, Ş. Ţălu, H. D. da Fonseca Filho, N. S. Ferreira, R. S. Matos, H. Zahrabi and L. Dejam, *Sci. Rep.*, 2022, **12**, 12002.
131 Ş. Ţălu, B. Astinchap, S. Abdolghaderi, A. Shafiekhani and I. A. Morozov, *Sci. Rep.*, 2020, **10**, 22266.
132 T. Wolkenstein, *Adv. Catal.*, 1960, **12**, 189–264.
133 C. Vogt and B. M. Weckhuysen, *Nat. Chem. Rev.*, 2022, **6**, 89–111.
134 J. Tyczkowski and H. Kierzkowska-Pawlak, *ACS Appl. Mater. Interfaces*, 2024, **16**, 37339–37345.
135 B. P. Mishra, J. Dahiya and V. Krishnan, *Chem. Commun.*, 2025, **61**, 17302–17329.
136 X. Zhang, L. Cheng, Y. Tian, Y. Zhang and S. Wang, *Chem. Commun.*, 2025, **61**, 11330–11352.
137 G. Zhang, Z. Wang and J. Wu, *Nanoscale*, 2021, **13**, 4359–4389.
138 Q. Li, X. Li, B. Zhang and B. Jiang, *Adv. Funct. Mater.*, 2025, **35**, 2506421.
139 F. Liao, B. T. W. Lo and E. Tsang, *Eur. J. Inorg. Chem.*, 2016, 1924–1938.
140 P. J. Jodłowski, R. J. Jędrzejczyk, A. Gancarczyk, J. Łojewska and A. Kołodziej, *Chem. Eng. Sci.*, 2017, **162**, 322–331.
141 H. Kierzkowska-Pawlak, P. Tracz, W. Redzynia and J. Tyczkowski, *J. CO2 Util.*, 2017, **17**, 312–319.
142 N. Mohammadpour, H. Kierzkowska-Pawlak, J. Balcerzak and J. Tyczkowski, *RSC Adv.*, 2024, **14**, 16758–16764.
143 H. Kierzkowska-Pawlak, L. Bilińska and J. Tyczkowski, *Ecol. Chem.Eng. S*, 2023, **30**, 489–504.
144 H. Kierzkowska-Pawlak, E. Kruszczak and J. Tyczkowski, *Appl. Catal., B*, 2022, **304**, 120961.
145 A. Kędzierska-Sar, M. Fronczak, M. Gmurek and L. Bilińska, *Molecules*, 2025, **30**, 969.
146 M. Bilińska, L. Bilińska, M. Fronczak, A. Kędzierska-Sar, H. Kierzkowska-Pawlak and M. Gmurek, *Sci. Rep.*, 2025, **15**, 18580.
147 A. Essakhi, A. Löfberg, S. Paul, B. Mutel, P. Supiot, V. Le Courtois, P. Rodriguez, V. Meille and E. Bordes-Richard, *Microporous Mesoporous Mater.*, 2011, **140**, 81–88.
148 C. Liang, L. Zhang, Y. Zheng, S. Zhang, Q. Liu, G. Gao, D. Dong, Y. Wang, L. Xu and X. Hu, *Fuel*, 2020, **262**, 116521.
149 X. Gao, P. Cai, Z. Wang, X. Lv and S. Kawi, *Top. Catal.*, 2023, **66**, 299–325.
150 W. Jiang, Y. Lin, C. Sun, Y. Sun and Y. Zhu, *Molecules*, 2024, **29**, 4618.
151 J. Coker, D. B. Afari, J. Narku-Tetteh and R. Idem, *Clean Energy*, 2019, **3**, 263–277.
152 X. Jin, C. Wu, L. Fu, X. Tian, P. Wang, Y. Zhou and J. Zuo, *J. Environ. Sci.*, 2023, **124**, 330–349.
153 S. Afandizadeh and E. A. Foumeny, *Appl. Therm. Eng.*, 2001, **21**, 669–682.
154 S. Mahmoudi and M. W. Hlawitschka, *ChemBioEng Rev.*, 2022, **9**, 63–92.
155 J. Tyczkowski, H. Kierzkowska-Pawlak, E. Kruszczak, L. Bilińska, M. Bilińska and M. Gmurek, *Eur. Pat.*, EP23215146.4, 2023.
156 B. A. T. Mehrabadi, S. Eskandari, U. Khan, R. D. White and J. R. Regalbuto, *Adv. Catal.*, 2017, **61**, 1–35.
157 I. U. Din, Q. Nasir, M. D. Garba, A. I. Alharthi, M. A. Alotaibi and M. Usman, *Mini-Rev. Org. Chem.*, 2022, **19**, 92–110.
158 S. Mehla, J. Das, D. Jampaiah, S. Periasamy, A. Nafady and S. K. Bhargava, *Catal. Sci. Technol.*, 2019, **9**, 3582–3602.
159 R. Balzarotti, M. Ambrosetti, M. Arnesano, A. Anglani, G. Groppi and E. Tronconi, *Appl. Catal., B*, 2021, **283**, 119651.
160 M. I. Domínguez, M. A. Centeno, M. Martínez, L. F. Bobadilla, Ó. H. Laguna and J. A. Odriozola, *Chem. Eng. Res. Des.*, 2021, **171**, 13–35.
161 C. Liu, M. Li, J. Wang, X. Zhou, Q. Guo, J. Yan and Y. Li, *Chin. J. Catal.*, 2016, **37**, 340–348.
162 S. Ferdous, U. R. Gracida-Alvarez, M. Ferrandon, M. Delferro, P. T. Benavides and M. Urgun-Demirtas, *Catal. Sci. Technol.*, 2025, **15**, 4419–4429.
163 F. G. Baddour, L. Snowden-Swan, J. D. Super and K. M. Van Allsburg, *Org. Process Res. Dev.*, 2018, **22**, 1599–1605.
164 D. Garg, P. B. Henderson, R. E. Hollingsworth and D. G. Jensen, *Mater. Sci. Eng. B*, 2005, **119**, 224–231.
165 W. Li, Y. Liu, M. Mu, F. Ding, Z. Liu, X. Guo and C. Song, *Appl. Catal., B*, 2019, **254**, 531–540.
166 D. Jampaiah, D. Damma, A. Chalkidis, P. Venkataswamy, S. K. Bhargava and B. M. Reddy, *Catal. Today*, 2020, **356**, 519–526.
167 C. Liang, H. Tian, G. Gao, S. Zhang, Q. Liu, D. Dong and X. Hu, *Int. J. Hydrogen Energy*, 2020, **45**, 531–543.
168 K. Li, X. Li, L. Li, X. Chang, S. Wu, C. Yang, Z. Song, J. Zhao and J. Gong, *JACS Au*, 2023, **3**, 508–515.
169 E. Spennati, G. Garbarino, P. Riani and G. Busca, *Int. J. Hydrogen Energy*, 2023, **48**, 25006–25015.
170 D. H. Kim, S. W. Han, H. S. Yoon and Y. D. Kim, *J. Ind. Eng. Chem.*, 2015, **23**, 67–73.
171 C. Y. Chou, J. A. Loiland and R. F. Lobo, *Catalysts*, 2019, **9**, 773.
172 L. Pastor-Pérez, M. Shah, E. Le Saché and T. Ramirez Reina, *Catalysts*, 2018, **8**, 608.
173 Z. Sun, J. Huang, L. Zhou and Y. Zhang, *Catal. Sci. Technol.*, 2025, **15**, 2964–2976.

